WIND TUNNEL INVESTIGATION OF THE AERODYNAMIC CHARACTERISTICS OF HIGH LIFT DEVICES ON SUPERSONIC WINGS AT LOW SUBSONIC SPEED

Thesis by

James E. Densmore

In Partial Fulfillment of the Requirements

For the Degree of

Aeronautical Engineer

California Institute of Technology

Pasadena, California

1949

ACKNOWLEDGEMENT

The author wishes to express his gratitude to Mr. Henry T. Nagamatsu for his helpful guidance and continued advice in the preparation of this thesis.

The author is also indebted to Mr. Philip G. Blenkush, co-worker in the experimental work, for his advice and assistance.

ABSTRACT

An investigation was made to determine the effect of various high lift devices on a highly sweptforward wing with a leading edge sweep angle of 55 degrees and on a straight wing, both wings having an aspect ratio of 1.72 and the same span.

Experimental tests were made in the Cal Tech - Merrill low speed wind tunnel at Pasadena City College on both types of wing with and without fuselage. High lift devices investigated were extended leading edge flaps, plain leading edge flaps, extended trailing edge flaps, and split flaps. Both 70 per cent and full span configurations were used in each case except for the plain leading edge flaps. All force data was reduced to standard non-dimensional lift, drag, and pitching moment coefficients, and the results presented in standard graphical form. In addition, photographs of tuft surveys were made for typical configurations.

The maximum lift coefficient obtained from the basic wings was approximately the same for both, but the angle of attack for maximum lift was appreciably lower for the straight wing than for the sweptforward wing.

The addition of the fuselage increased the maximum lift coefficient of both the basic wings and of the sweptforward wing with flap configurations, but the fuselage was detrimental to the lift for the straight

wing with flap configurations.

Straight wing configurations gave respectively higher maximum lift coefficients and larger lift curve slopes than on the comparable sweptforward wing models. All high lift devices investigated were more effective on the straight wing than on the sweptforward wing.

Extended trailing edge flaps were the most effective of the flaps investigated in increasing the maximum lift, but gave the largest negative increase in the pitching moments.

On the straight wing the 70 per cent span split and 70 per cent span extended trailing edge flaps at optimum flap deflection angles gave a higher maximum lift coefficient than the full span flaps at the optimum flap deflection. When the straight wing was mounted on the fuselage, this effect was true only for the split flaps.

TABLE OF CONTENTS

I. INTRODUCTION

In the past few years, radical changes in the configuration of airplanes have been necessitated for transonic and supersonic flight. At the present time a thin airfoil section with little or zero camber, sweptforward or sweptback plan form, and a sharp leading edge seems desirable from a transonic and supersonic aerodynamic point of view. To accomplish this design with an efficient structure, a low aspect ratio wing is required.

It is well known that the maximum lift coefficient is low for a thin wing with zero camber and a sharp leading edge at subsonic speeds. Decreasing the aspect ratio decreases the lift curve slope and increases the angle of attack for maximum lift. Thus, for airplanes or missiles designed for supersonic flight, there is a real difficulty in obtaining sufficient lift for low subsonic speed conditions such as landing. Additional aerodynamic problems are introduced by a highly swept wing, a configuration desirable for high speed flight.

The object of this investigation was to obtain systematic results for various high lift devices on supersonic airplane configurations at low subsonic speeds. Reported in Ref. 1 are results of an investigation on a delta wing and a highly sweptback wing, both having leading edge sweepback angles of 65 degrees. As a

continuation of that program, this investigation was made on a highly sweptforward wing and a straight wing, both having the same low aspect ratio. Wings alone and in combination with a fuselage compatible for supersonic airplane or missile design were investigated.

II. DESCRIPTION OF EQUIPMENT AND MODELS

The wind tunnel utilized for this investigation was the low speed 2-foot by 4-foot Cal Tech - Merrill wind tunnel located at Pasadena City College. This tunnel operates at a maximum dynamic pressure of 13.5 pounds per square foot (approximately 80 miles per hour). Force measurements were made on the three component balance system generally used in this tunnel. The models were supported upright on two struts to the wing trunnions and a third support strut to the rear. For the swept-forward wing, the rear support strut was attached to a trunnion located on the centerline near the trailing edge. For the straight wing, the rear support strut of the balance system was attached to a brass sting extending aft from the trailing edge. When the wings were tested with the fuselage, the rear trunnions were situated inside the fuselage.

The sweptforward wing tested was a mahogany model previously constructed according to a supersonic tailless airplane design by Frank Dore (Cf. Ref. 2). Because of the symmetry of the model, which was originally designed with a sweptback configuration, it was feasible to turn the wing around for this sweptforward investigation. The wing had a double wedge symmetrical airfoil section with the maximum thickness at the 50 per cent chord point.

Considering the chord as being measured parallel to the direction of flight, the maximum thickness of the wing was 5 per cent of the chord at the root section and 2 per cent at the tip. The wing had a leading edge sweepforward of 55 degrees, giving the 50 per cent chord line a sweepforward of 61 degrees (Cf. Fig. 1). The characteristics of the wing were: an aspect ratio of 1.72, a taper ratio of 0.513, an area of 98.35 square inches, and a span of 13 inches.

The original wing was equipped with ailerons for the sweptback configuration. These ailerons were utilized as plain leading edge partial span flaps.

The straight wing model (Cf. Fig. 2) was constructed out of mahogany. The wing had a double wedge symmetrical airfoil section with the maximum thickness at the 50 per cent chord. The maximum thickness at the root chord was 5 per cent and at the tip, 3 per cent. The characteristics of the wing were: an aspect ratio of 1.72, a taper ratio of 0.5, an area of 98.35 square inches, and a span of 13 inches. The 50 per cent chord line had no sweep.

It is seen that the sweptforward wing and the straight wing have the same area, aspect ratio, and span.

As well as being tested alone, both wings were mounted on the fuselage as shown in Figs. 3 and 4 for wing plus fuselage tests. However, the fuselage was re-worked to

provide an alternate nose piece giving a configuration representative of a rocket propelled vechicle. Thus, in addition to the original nose a conical nose 5.6 inches long and having an apex angle of 30 degrees was investigated (Cf. Fig. 3).

The horizontal tail surfaces (Cf. Fig. 5) were provided to obtain preliminary information on the static longitudinal stability characteristics of the wing and body combinations. These tail surfaces were attached at two different heights on the vertical fin, 1.84 inches and 3.68 inches above the fuselage centerline, and were tested as sweptforward and sweptback tail surfaces. They were made of 0.040 inch dural sheet and had an area of 18.2 square inches. The aspect ratio was 1.50, and the leading edge sweepback angle was 65 degrees in the sweptback configuration.

Extended leading edge flaps, extended trailing edge flaps, and split flaps were tested on both wings alone and on both wings in combination with the fuselage. These flaps were fabricated from 0.020 phosphorous bronze sheet stock and were secured in place on the model with Scotch tape. Deflection angles of the split flaps were maintained with clay supports. In addition to these flaps, plain leading edge partial span flaps located at the wing tips were tested on the sweptforward wing.

Dimensions of the various flaps are given in the Code of Model Configurations on page 22 of this report.

III. TEST PROGRAM

Tests were made on both basic wings alone and on both basic wings mounted on the fuselage. Full span and partial span tests were made with extended leading edge flaps, extended trailing edge flaps, and split flaps mounted on the wings alone and on the wing-fuselage configurations. The angle of attack increments for the force tests varied from 2 degrees for the basic wings alone to 4 to 8 degrees for the other runs. The angle of attack range for practically all the runs was from zero through the stall.

All tests were made at a constant wind tunnel power setting corresponding to a dynamic pressure of about 11.0 pounds per square foot. Based on the mean aerodynamic chord and a dynamic pressure of 11.0 pounds per square foot, the Reynold's number was approximately 390,000 for both wings.

Tuft studies were made on several representative model configurations. Photographs were taken of tufts attached to the upper surface of the wings at angles of attack ranging from zero through the stall. In each case the angle of attack increments were determined by an observed definite change in the flow pattern.

IV. DISCUSSION OF CORRECTIONS

Since the primary purpose of the investigation was to determine relative effects of various modifications rather than any absolute force measurements, no tunnel wall corrections were made.

No attempt was made to determine the effect on drag of the interference between support struts and model. However, a tare drag coefficient of the support struts based on the wing area of the models, as determined in Ref. 1, was subtracted as a constant term from all model drag coefficients over the entire angle of attack range. This value was $C_{D_T} = 0.010$.

As may be determined from Fig. 7, the zero lift angles are not equal to zero but are equal to one degree. This is contradictory to what would be expected for symmetrical airfoils, but is in agreement with the zero lift angles reported in Ref. 1. It seems best to conclude, as was done in Ref. 1, that there is a flow inclination in the test section of the wind tunnel.

All force and moment coefficients for both wings and wing-fuselage configurations were calculated about the aerodynamic center as determined from the average slope of the moment curve near zero lift for the wing alone. The aerodynamic center was at 0.372 of the mean

aerodynamic chord for the sweptforward wing W_s and 0.182 of the mean aerodynamic chord for the straight wing W.

The trailing portions of the models approached rather close to the floor of the tunnel because of the large angle of attack range necessary. This may have affected measurements made at high angles of attack, especially when the wings were mounted on the fuselage.

V. RESULTS AND DISCUSSION

The results of the force measurements were reduced to standard non-dimensional lift, drag, and pitching moment coefficients and plotted in Figs. 7 through 31. The maximum lift coefficient for each flap was plotted against flap angle deflection and the results form the summary curves in Figs. 32 and 33. It should be noted in connection with the summary curves, that the results gave fairly flat curves for the sweptforward wing configurations and sharper peaked curves for the straight wing configurations. Representative stall patterns are shown in the tuft photographs, Figs. 34 through 46.

In the discussion which follows, consideration of the slope of the lift curves is to be interpreted as applying to that portion of the curve in the lower angle of attack range. Similarly, stability considerations apply to the lower angle of attack range for the respective curves considered.

Compared in Fig. 7 are the characteristics of the two basic wings. The maximum lift coefficient is about the same for both wings, but the attitude for maximum lift of the straight wing is appreciably less than that for the sweptforward wing, and the lift curve slope is

appreciably greater for the straight wing than for the sweptforward wing. Comparing the two basic wings with results presented in Ref. 1, it is seen that the lift curve slopes for the sweptback and delta wings nearly match that of the straight wing used in this investigation. However, the maximum lift coefficients for the wings used in Ref. 1 were appreciably higher and occurred at higher angles of attack.

The force measurement results obtained for the basic wings mounted on the fuselage are presented in Fig. 8. The addition of the fuselage on both wings increased the maximum lift coefficient by about 0.26, increased the angle of attack for maximum lift, increased the lift curve slope slightly, and had a destabilizing effect on the models. The addition of the fuselage also changed the shape of the lift curve peak, particularly for the straight wing. In comparison, this same fuselage increased the maximum lift coefficient by 0.12 on the sweptback wing used in Ref. 1, whereas it decreased the maximum lift coefficient by 0.12 on the delta wing and gave no significant change in either the shape of the lift curve peaks or the attitude for maximum lift for the two wings investigated in Ref. 1.

The effectiveness of the horizontal tail surfaces used in this investigation may be seen in Figs. 9 and 10.

The tail tends to stabilize the pitching moment curves somewhat, the amount depending on the tail location and configuration. The best stabilizing effect was obtained from the sweptback tail located in the higher position.

The effect of the conical nose is shown in Fig. 10 for the straight wing-fuselage combination. The conical nose was also tested with the sweptforward wing-fuselage combination, and no noticeable changes were observed for both wings over the results obtained when the ducted fuselage was tested.

As shown in Fig. 11, the partial span plain leading edge flaps had very little effect on the basic sweptforward wing curves except for the radical change in the shape of the lift curve at attitudes above the angle of attack for maximum lift. This same change in the shape of the lift curve peak was observed for all flaps investigated on the sweptforward wing.

It is seen in Figs. 12, 13 and 14, that extended leading edge flaps gave a slight increase in the maximum lift coefficient, but no more than can be attributed to the increase in wing area due to the addition of the flaps. The slope of the moment curves was changed in a destabilizing sense. The 70 per cent span flaps showed the same effects, but less pronounced.

As shown in Figs. 15, 16 and 17, the split flaps

gave a typical increase in lift at a given attitude with no change in the slope of the lift curve. A negative increase in the moment coefficient and a slight stable change in the slope of the moment curve was also observed. Reducing the span of the flaps reduced the magnitude of the effects of the flaps.

The extended trailing edge flaps gave the largest increase in maximum lift coefficient and the largest lift curve slope of all the flaps investigated on the sweptforward wing. But, as is shown in Figs. 18, 19 and 20, the negative pitching moment coefficients are also larger than for the other configurations. Therefore, some of the high lift obtained from the extended trailing edge flaps would be lost due to tail loads necessary to trim the diving moment. Higher negative pitching moments were obtained for the 70 per cent span flaps than for the full span flaps, and the angle of attack for maximum lift was increased by reducing the flap span.

Three general characteristics were observed in the moment curves for the straight wing with flap configurations. Whereas in the sweptforward wing with flaps the moment coefficient increased negatively quite rapidly in the higher angle of attack region, the moment coefficient for the straight wing, in general reached a negative maximum at an angle of attack near the maximum

lift and then showed little variation at attitudes above the angle of attack for the maximum lift. The second characteristic was that the maximum lift was obtained at a lower angle of attack for the straight wing than for the sweptforward wing with the same flap configuration. It is quite true in general that the slope of the lift curve for the straight wing configurations is larger than for a comparable sweptforward wing configuration. The third trend observed was that the addition of the fuselage did not increase the lift of the straight wing with flap configurations as it did in the case of the sweptforward wing.

As is observed by comparing Figs. 21 and 22 with Fig. 7, extended leading edge flaps on the straight wing did not change the slope of the lift curve over that for the basic wing; but the flaps did increase the maximum lift; and the attitude for maximum lift was increased. The model was less stable with flaps, particularly at higher angles of attack. By comparing Fig. 23 with Fig. 8, it is seen that extended leading edge flaps on the straight wing with fuselage did not change the slope of the lift curve, but did change the shape of the lift curve near the peak. The attitude for maximum lift was decreased. The model was more stable with the flaps.

When split flaps were tested on the straight wing, a typical shift for this type of flap resulted in the lift curve (Cf. Figs. 24 and 25). The attitude for maximum lift was decreased slightly over that for the basic wing. The flaps had a slightly destabilizing effect on the model. Full span, 12.5 per cent chord flaps were tested with results which were nearly the same as for the 25 per cent chord flaps. The 12.5 per cent chord flaps had a destabilizing effect as did the larger split flaps, but the negative shift in the moment curve was not as great as for the 25 per cent chord flaps. The 70 per cent span, 25 per cent chord split flaps with a 20 degree flap deflection gave the same maximum lift at the same attitude as the full span flaps, with a larger slope in the lift curve (Cf. Fig. 26). The partial span flaps with 40 degree flap deflection had a higher maximum lift at a one degree higher angle of attack than the full span split flaps with the same flap deflection. The slope of the moment curve was the same for the partial and full span flaps, but the negative shift in the moment curve was less for the partial span flaps.

With reference to Figs. 28, 29 and 30, extended trailing edge flaps gave a typical shift in the lift curve. The maximum lift coefficient was more than doubled by the addition of the flaps, and the angle of attack

for the maximum lift was nearly the same. The flaps had a stabilizing effect on the moment curve and produced a large negative shift in the moment coefficients. Full span, 15 per cent chord extended trailing edge flaps were tested with the same effects observed as with the larger flaps, but not quite as pronounced. Neither was the negative shift in the moment curve as great. Seventy per cent span extended trailing edge flaps slightly increased the maximum lift coefficient over that found for the full span flaps, with a large increase in the angle of attack for maximum lift. An abrupt stall was found to occur with the partial span flaps. Reducing the span reduced the negative shift in the moment curve for this type of high lift device.

VI. CONCLUSIONS

The results of the low speed tests on the low aspect ratio highly sweptforward wing and the comparable straight wing used in this investigation indicate the following:

1. When tested with the fuselage, the sweptforward and straight wings had a higher maximum lift coefficient than when they were tested alone.

2. For any given straight wing model configuration, the slope of the lift curve was greater than for the comparable sweptforward configuration.

3. All high lift devices investigated were more effective on the straight wing than on the sweptforward wing.

4. The maximum lift coefficient obtained from the respective flap configurations investigated was higher on the straight wing alone than on the straight wing with comparable flap configurations mounted on the fuselage.

5. The increase in maximum lift was the same for a given flap mounted on the sweptforward wing alone as for the same flap mounted on the sweptforward wing with fuselage.

6. The extended leading edge flaps gave an

increase in the unstable sense to the slope of the pitching moment curve and were the least effective in increasing lift.

7. Extended trailing edge flaps gave the largest increase in lift of the flaps investigated and gave the largest negative increase in the pitching moment coefficient.

8. For both the split and extended trailing edge flaps at optimum deflection on the straight wing, the 70 per cent span flaps gave a higher maximum lift coefficient than the full span flaps. When the fuselage was added, this effect was true only for the split flaps.

9. Curves of maximum lift coefficient plotted against flap deflection were flat for the sweptforward wing, but the maximum lift coefficient decreased rapidly from the value at the optimum flap deflection angle for the straight wing configurations.

REFERENCES

1. Jensen, Arnold A., and Koerner, Warren G.: Wind Tunnel Investigation of a Supersonic Tailless Airplane at Low Subsonic Speed. Thesis, California Institute of Technology (1948).

2. Dore, Frank: The Design of Tailless Airplanes. Thesis, California Institute of Technology (1947).

INDEX OF FIGURES

	Figure Number
Tuft Studies	
W	34, 35
WB_1V	36, 37
W_s	38, 39
W_sB_1V	40
W_sF_3 [40]	41
WF_8 [40]	42, 43
$WF_8(70)$ [40]	44, 45, 46

CODE OF MODEL CONFIGURATIONS

The number in parenthesis following the flap designation refers to the portion of the wing span in per cent over which the flap extends. Omission of the number designates full span flaps. Except in the F_1 configuration, partial span flaps extended over the inboard portion of the wing. For wing-fuselage combinations, the flaps terminated at the fuselage; but the per cent span notation is as if the flaps were continuous over the inboard portion of the wing. The superscript on the flap configurations indicates flap angles in degrees as shown in Fig. 6. Thus $F_3(70)^{20}$ indicates a 70 per cent span 30 per cent chord extended trailing edge flap on W_s deflected 20 degrees.

W_s Basic sweptforward wing

W Basic straight wing

B_1 Circular fuselage with full length air duct

B_2 Circular fuselage with solid conical nose piece

V Vertical sweptback tail, area = 9.83 square inches, sweepback = 65 degrees, aspect ratio = 0.64, taper ratio = 0.63

H_1 Horizontal sweptback tail, area = 18.2 square inches, sweepback = 65 degrees, aspect ratio = 1.50, taper ratio = 0.74, mounted 1.84 inches above the fuselage axis on the vertical tail

H_2 Same as H_1 except mounted 3.68 inches above the fuselage axis on the vertical tail

H_3 Same as H_2 except sweptforward

F_1 Plain partial span leading edge flaps located at wing tip on W_s, 34 per cent span, 25 per cent chord

F_2 Split flap used on W_s, 25 per cent chord

F_3 Extended trailing edge flap used on W_s, 30 per cent chord

F_4 Split flap used on W_sB_1V, 25 per cent chord

F_5 Extended trailing edge flap used on W_sB_1V, 30 per cent chord

F_6 Split flap used on W, 25 per cent chord

F_7 Split flap used on W, 12.5 per cent chord

F_8 Extended trailing edge flap used on W, 30 per cent chord

F_9 Extended trailing edge flap used on W, 15 per cent chord

F_{10} Split flap used on WB_1V, 25 per cent chord

F_{11} Extended trailing edge flap used on WB_1V, 30 per cent chord

K_1 Extended leading edge flap used on W_s, 10 per cent chord

K_2 Extended leading edge flap used on W_sB_1V, 10 per cent chord

K_3 Extended leading edge flap used on W, 10 per cent chord

K_4 Extended leading edge flap used on WB_1V, 10 per cent chord

FIG. 1 SWEPTFORWARD WING

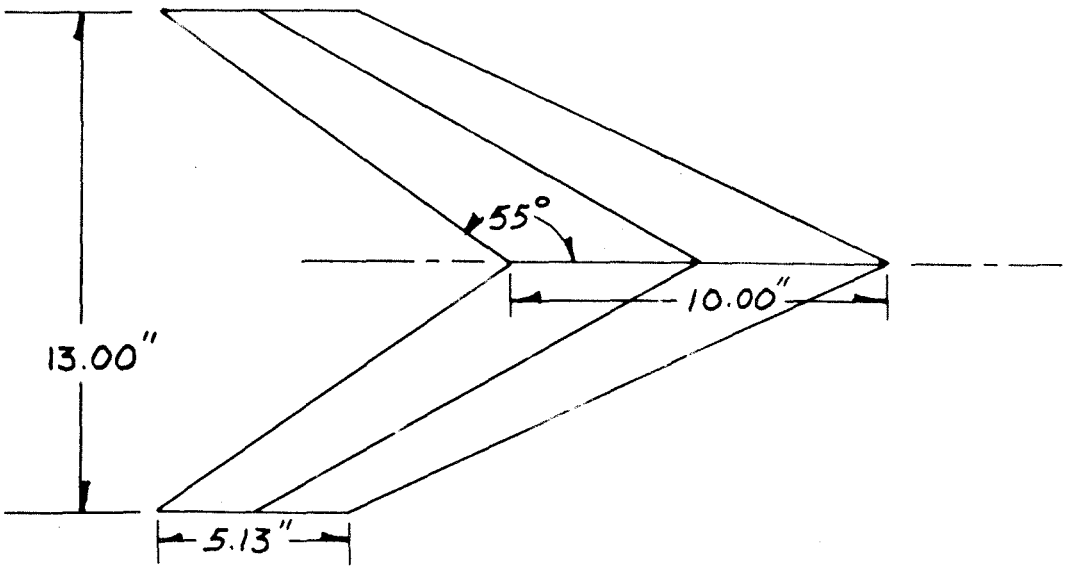

Root Chord: 5% thickness symmetrical double wedge section; maximum thickness located at .5 chord.
Tip Chord: 2% thickness symmetrical double wedge section.

FIG. 2 UNSWEPT WING

Root Chord: 5% thickness symmetrical double wedge section.

Tip Chord: 2% thickness symmetrical double wedge section.

Maximum thickness located at .5 chord.

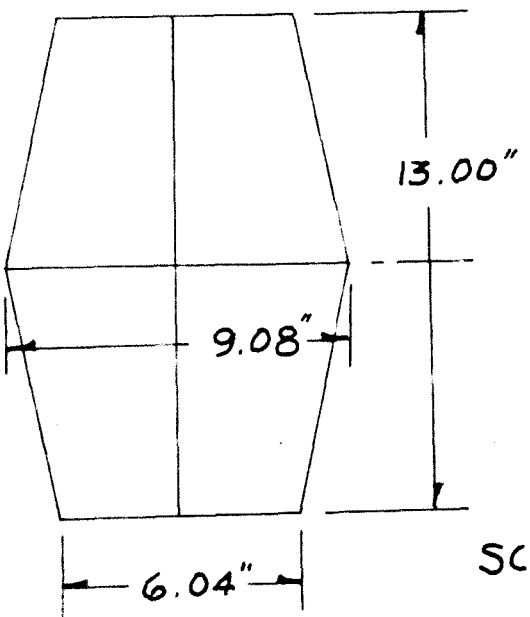

SCALE: $\frac{1}{5}$" = 1"

FIG. 3

SWEPTFORWARD WING AND FUSELAGE

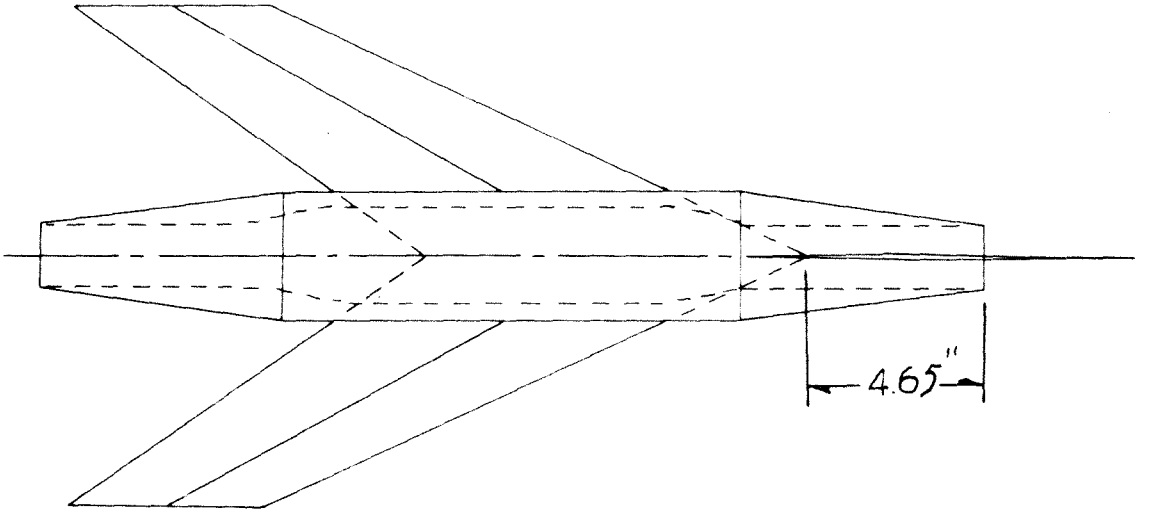

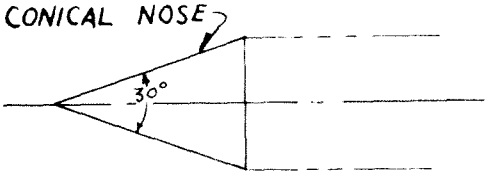

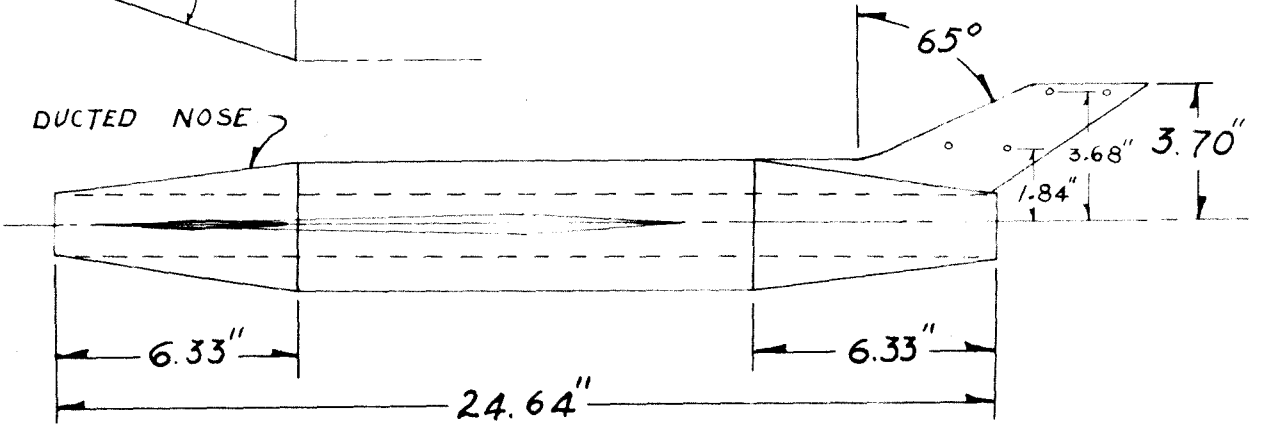

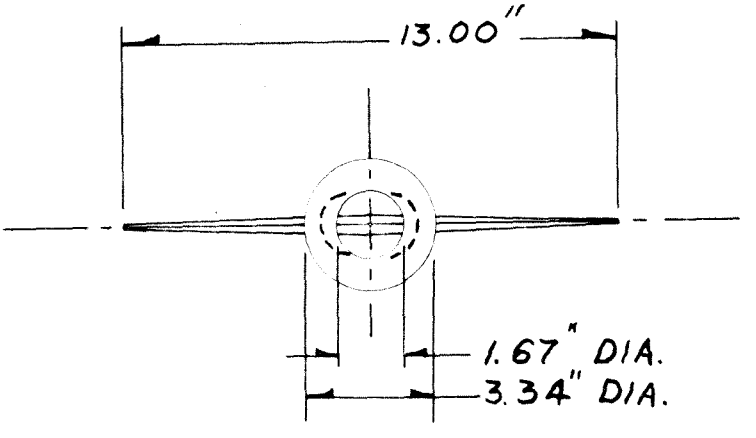

WING INCIDENCE = 0°

SCALE: $\frac{1}{5}$" = 1"

FIG. 4 UNSWEPT WING AND FUSELAGE

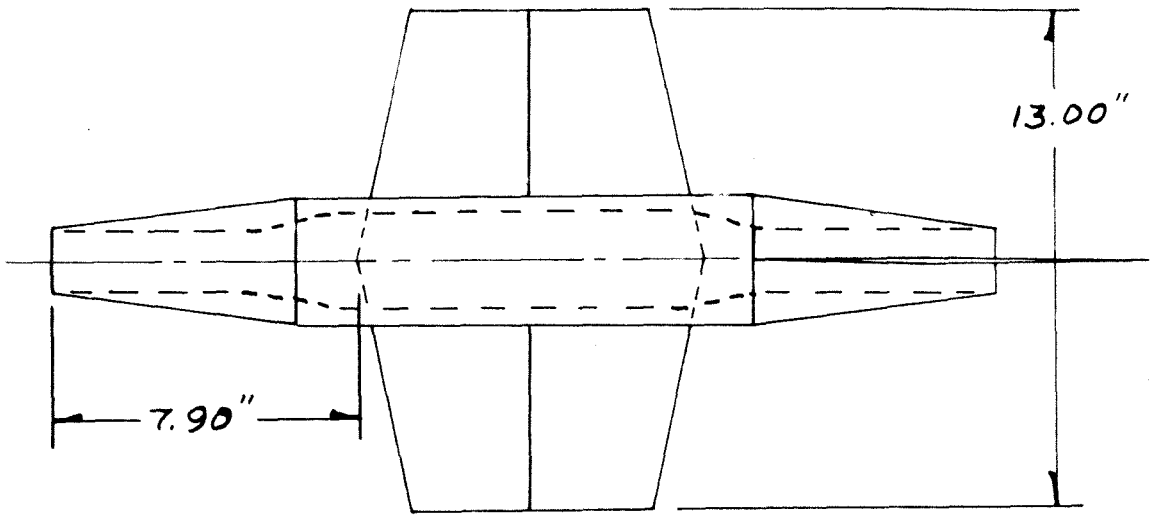

WING INCIDENCE = 0°

SCALE: $\frac{1}{5}$" = 1"

FIG. 5 HORIZONTAL TAIL

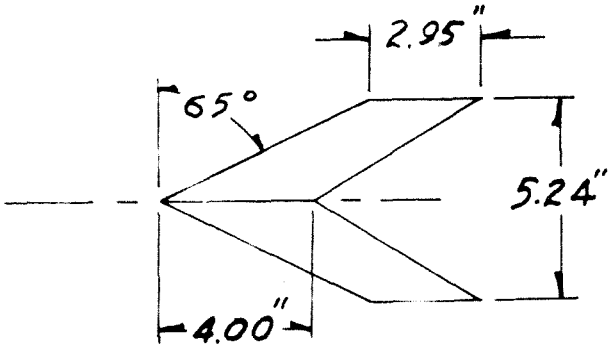

FIG. 6
FLAP ANGLES

EXTENDED LEADING EDGE FLAPS

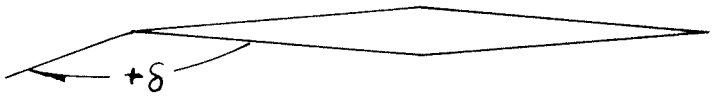

EXTENDED TRAILING EDGE FLAPS

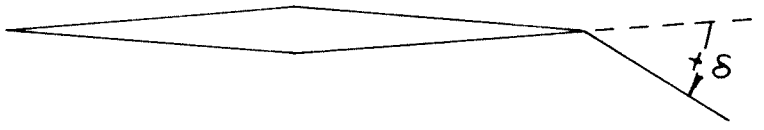

SPLIT FLAPS

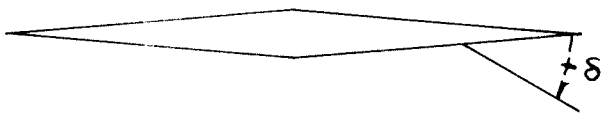

PLAIN LEADING EDGE FLAPS

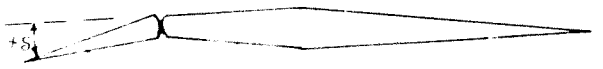

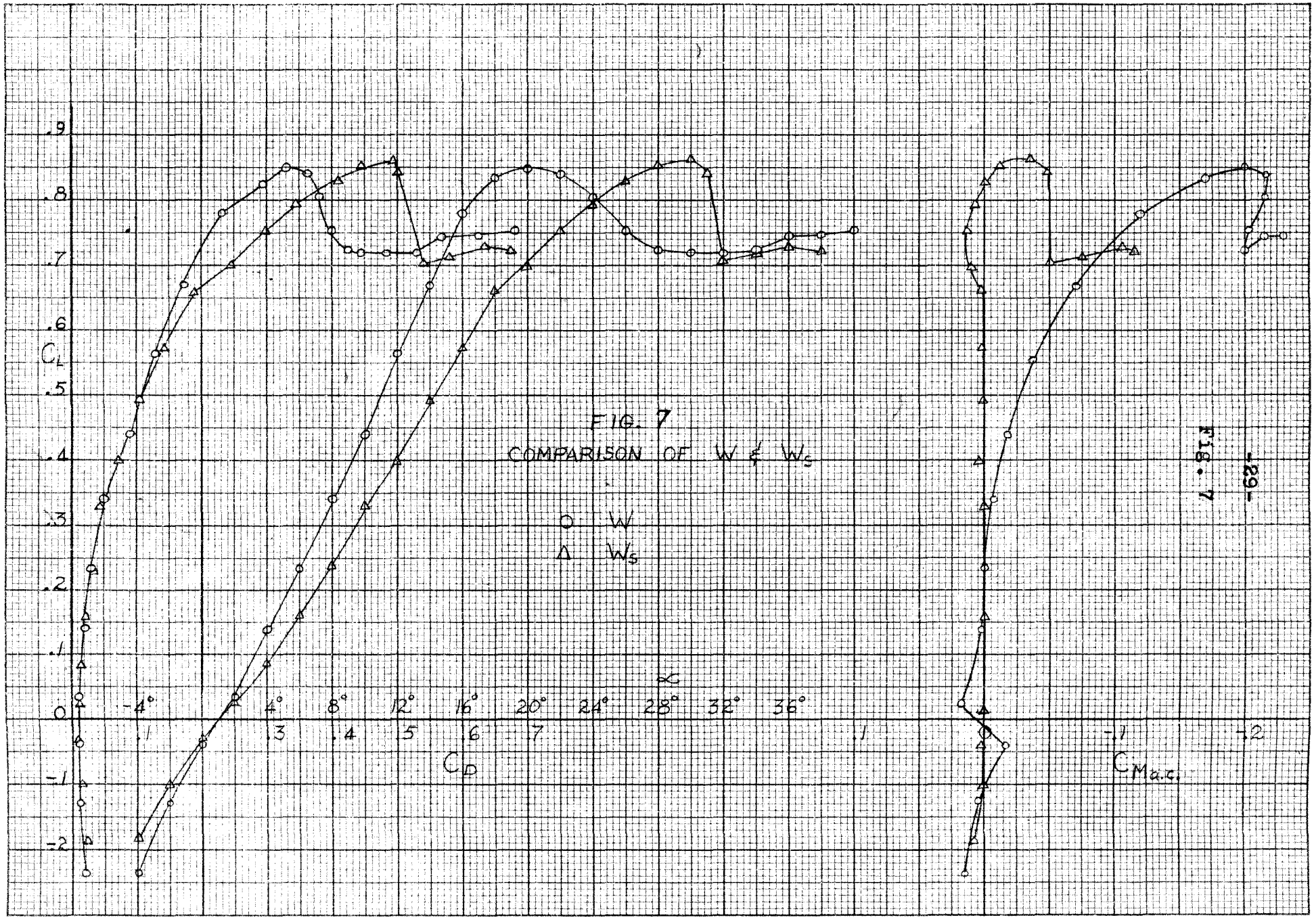

FIG. 7
COMPARISON OF W & W_s

○ W
△ W_s

Fig. 7

Fig. 8

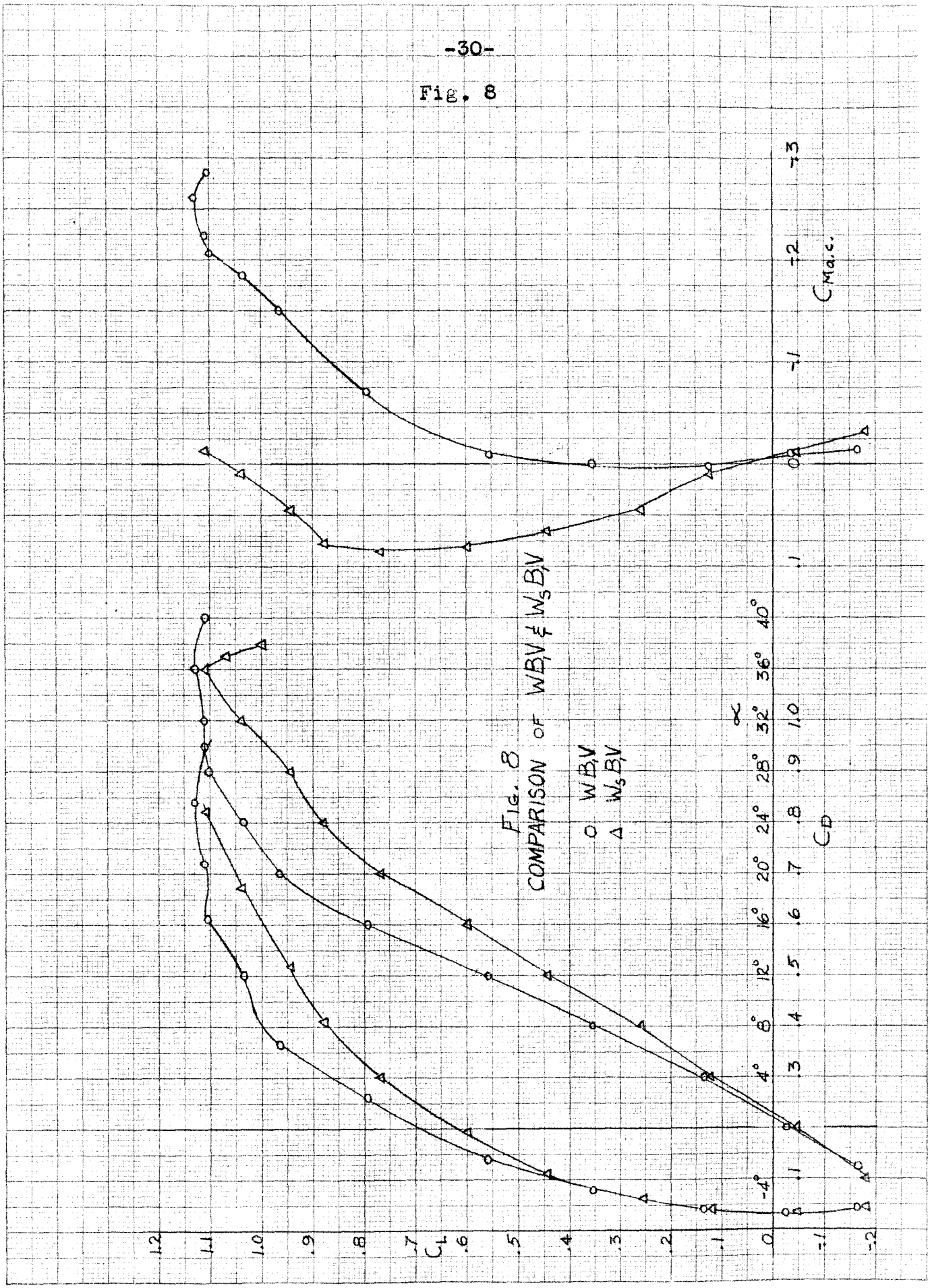
FIG. 8
COMPARISON OF WBV & WSBV
○ WBV
△ WSBV
CL
CD
Cm.a.c.
-4°
0°
4°
8°
12°
16°
20°
24°
28°
32°
36°
40°

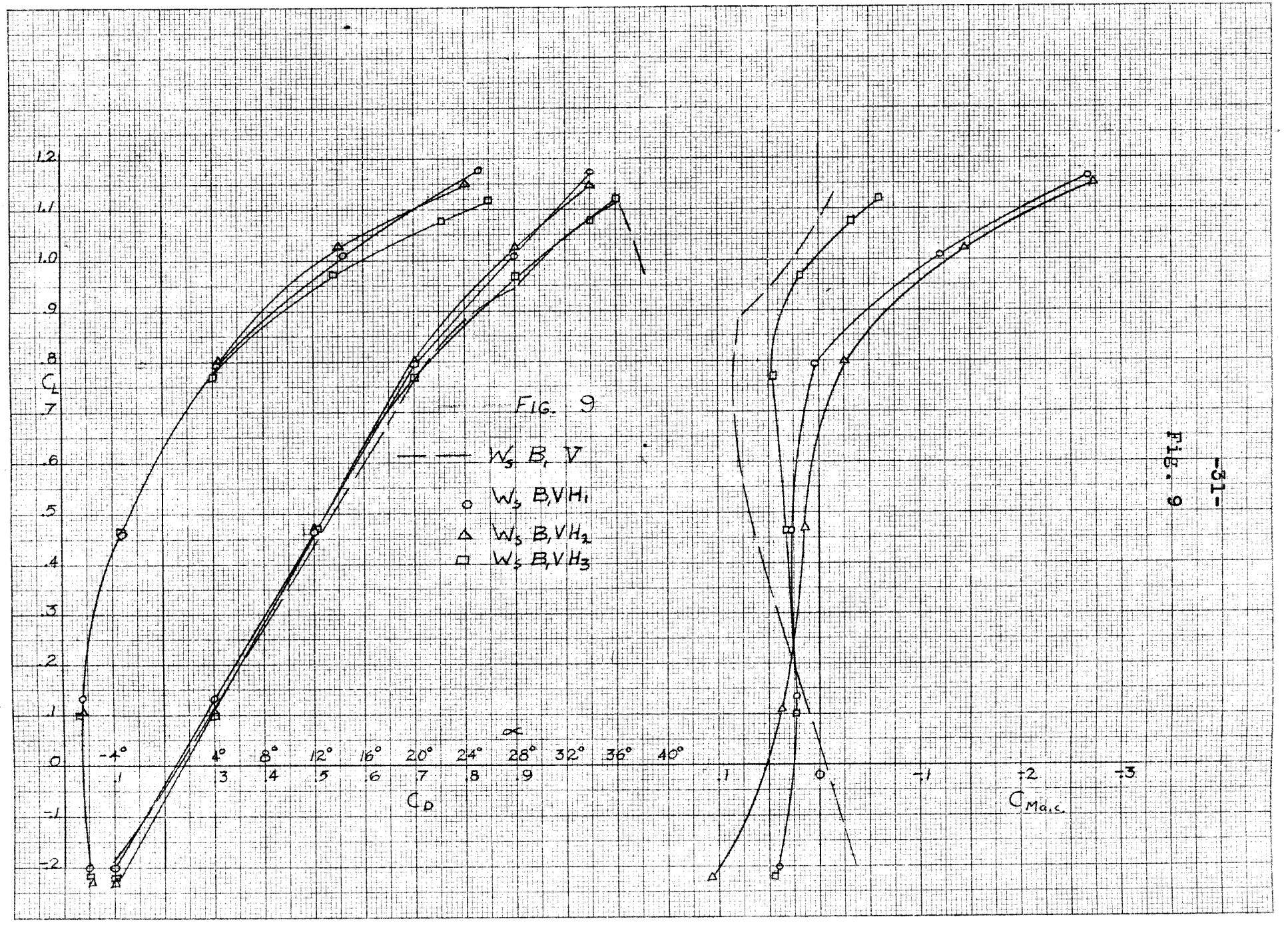
1.2
1.1
1.0
.9
.8
C_L
.7
.6
.5
.4
.3
.2
.1
0
-1
-2
-4°
4°
8°
12°
16°
20°
24°
28°
32°
36°
40°
α
.1
.3
.4
.5
.6
.7
.8
.9
C_D
.1
0
-.1
+.2
+.3
$C_{M_{a.c.}}$
W_5 B, V
W_5 B, V H_1
W_5 B, V H_2
W_5 B, V H_3

FIG. 9

Fig. 9

Fig. 10

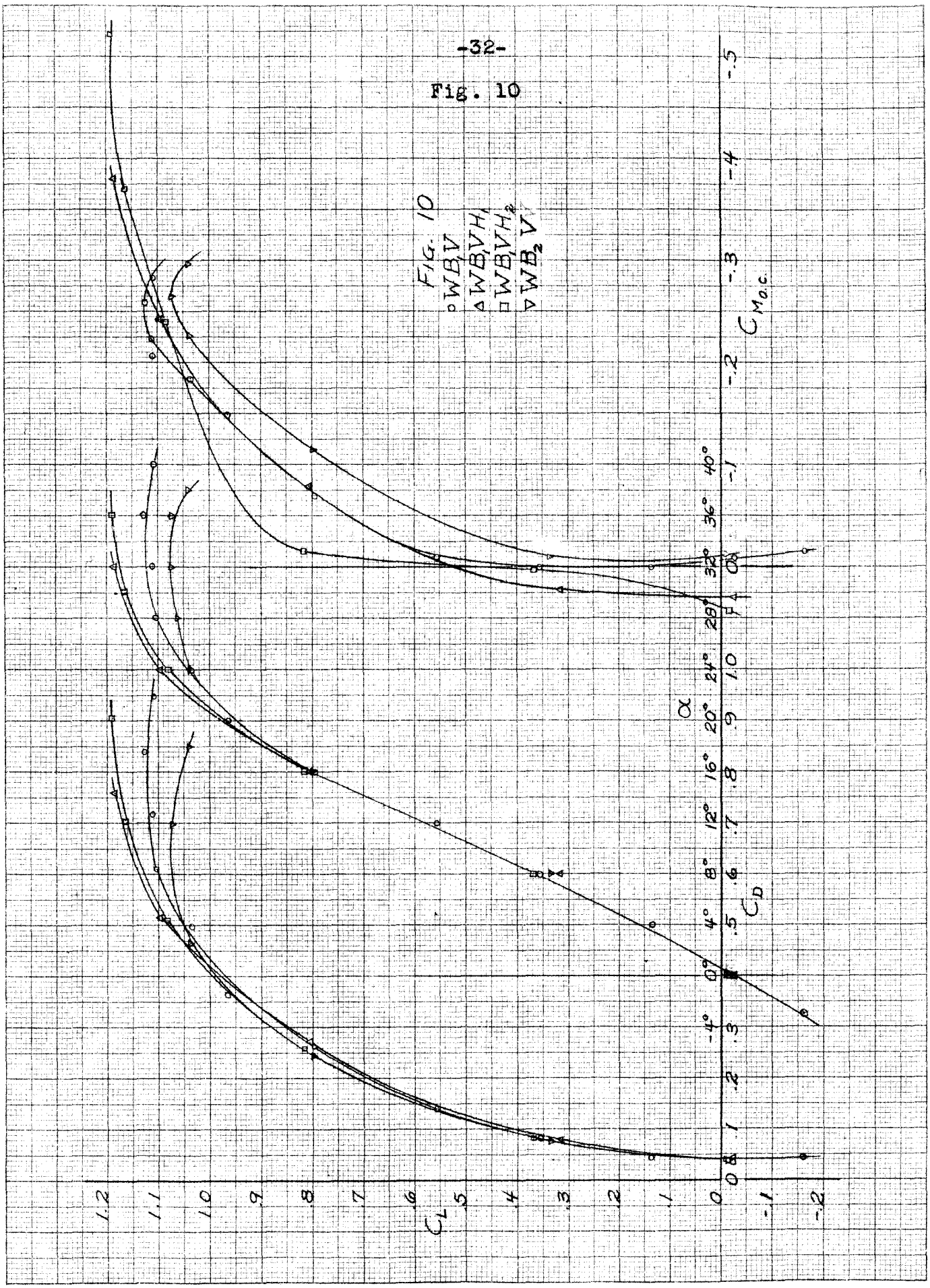

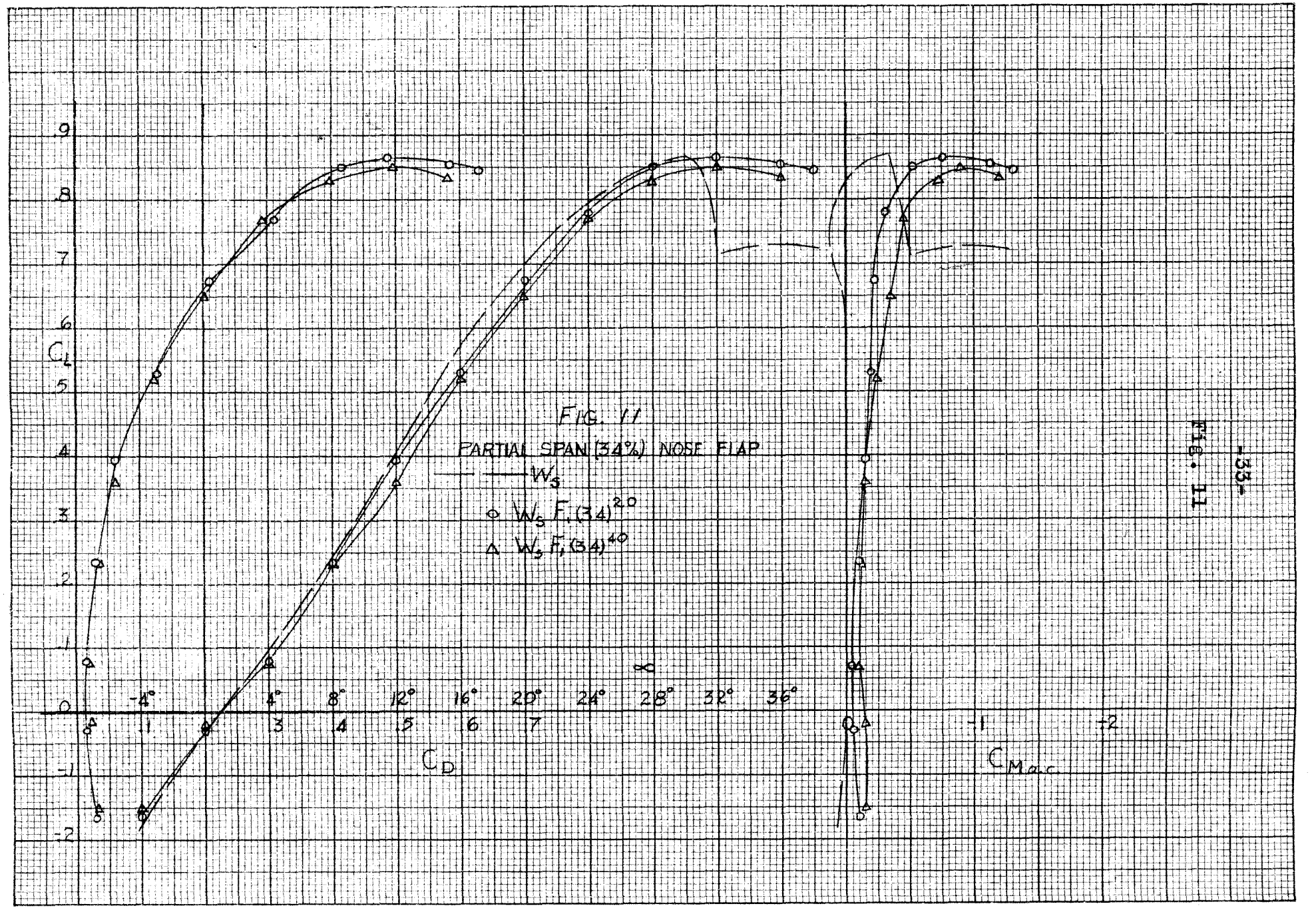
FIG. 11
PARTIAL SPAN (34%) NOSE FLAP
W_s
$W_s F_1(34)^{20}$
$W_s F_1(34)^{40}$
C_L
C_D
$C_{M_{a.c.}}$
α
-4°
0°
4°
8°
12°
16°
20°
24°
28°
32°
36°
.9
.8
.7
.6
.5
.4
.3
.2
.1
0
-.1
-.2
.1
.2
.3
.4
.5
.6
.7
-.1
-.2

Fig. 11

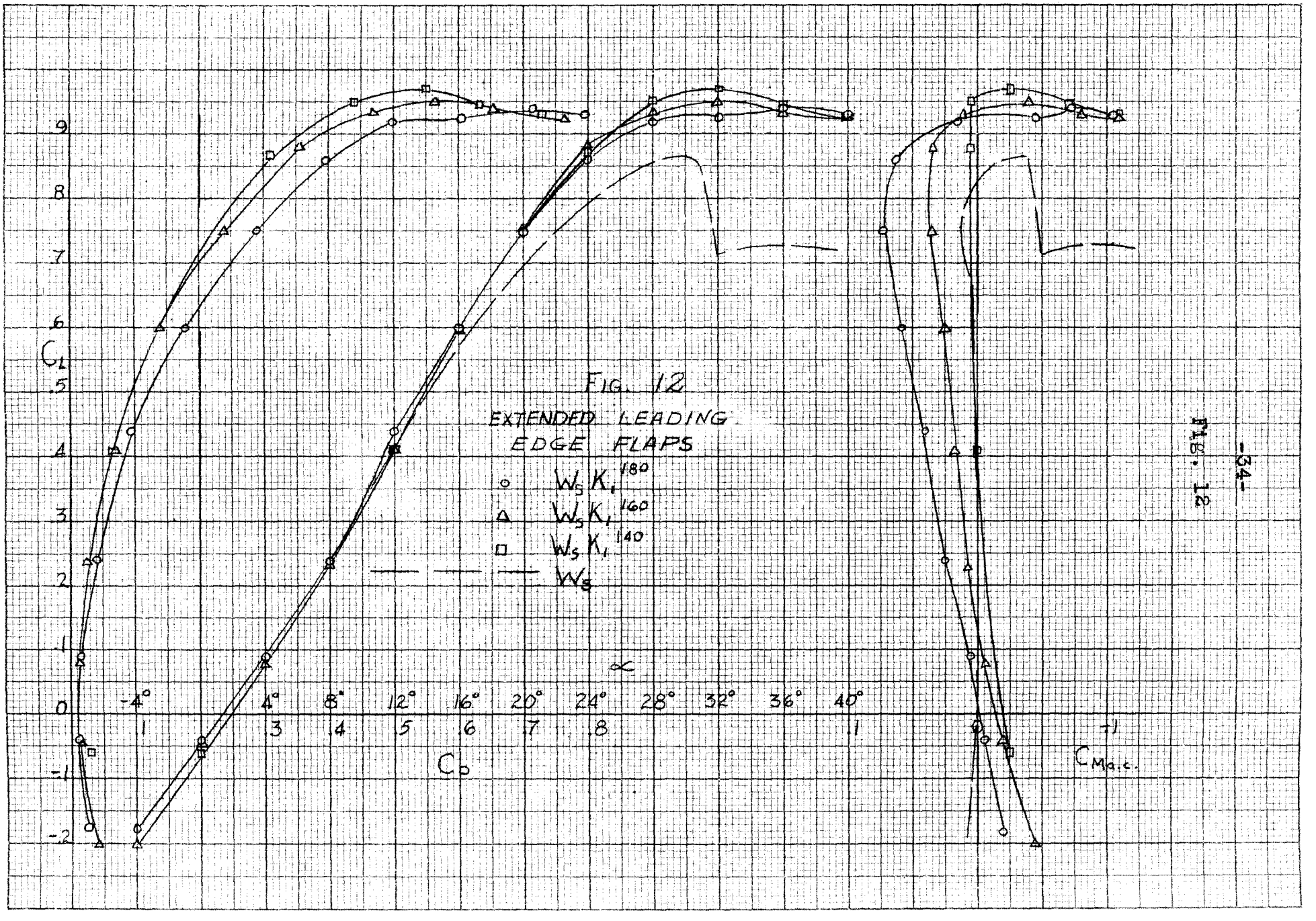
FIG. 12
EXTENDED LEADING EDGE FLAPS
$W_S K_1^{180}$
$W_S K_1^{160}$
$W_S K_1^{140}$
W_S
C_L
C_D
$C_{M_{a.c.}}$
α
-4°
4°
8°
12°
16°
20°
24°
28°
32°
36°
40°

FIG. 12

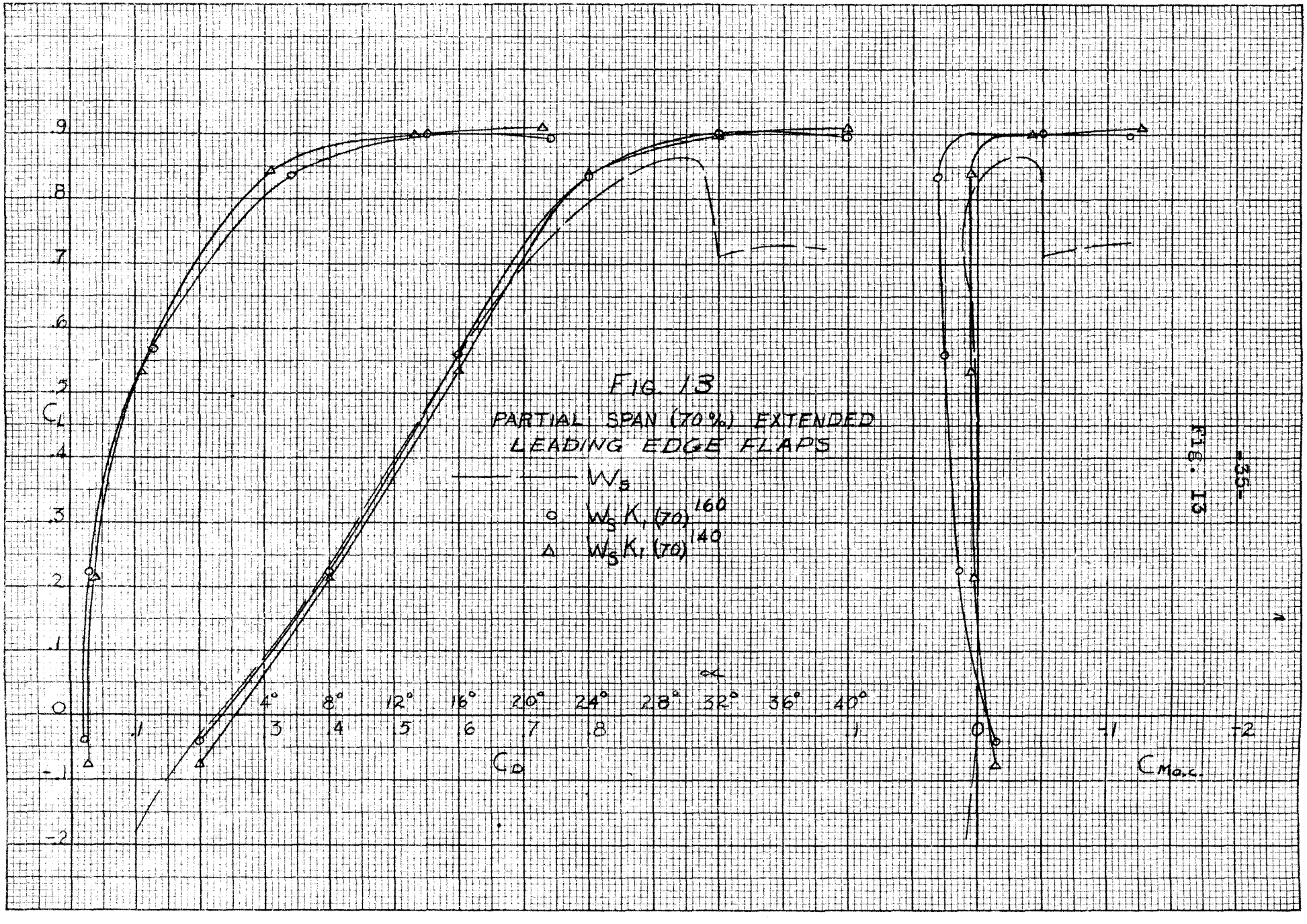
FIG. 13
PARTIAL SPAN (70%) EXTENDED LEADING EDGE FLAPS
W_S
$W_S K_1 (70)^{160}$
$W_S K_1 (70)^{140}$
C_L
C_D
$C_{M_{a.c.}}$
α
4° 8° 12° 16° 20° 24° 28° 32° 36° 40°
.9 .8 .7 .6 .5 .4 .3 .2 .1 0 -.1 -.2
.1 .3 .4 .5 .6 .7 .8
.1 0 -.1 -.2
FIG. 13
-35-

Fig. 14

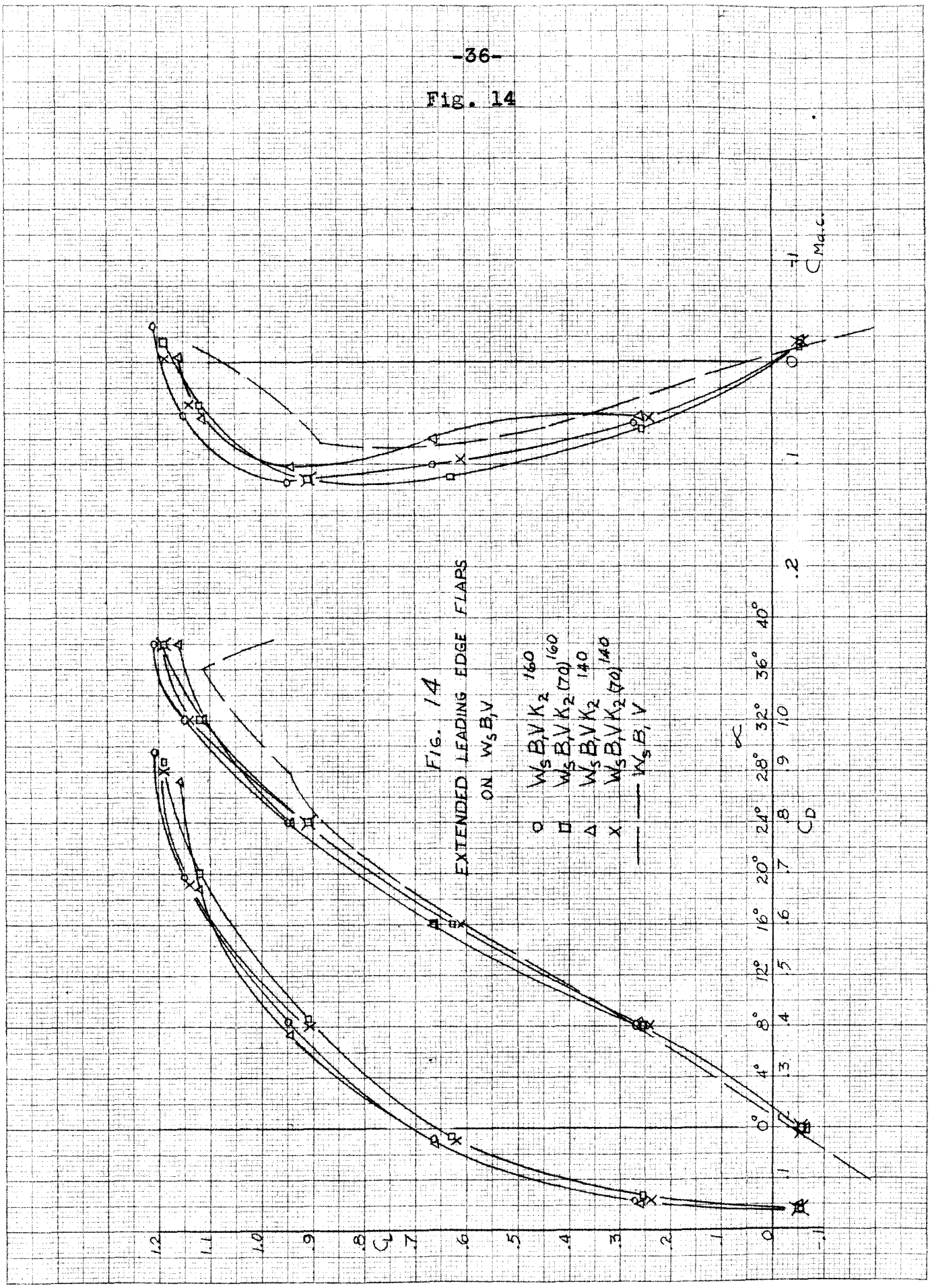
EXTENDED LEADING EDGE FLAPS
ON $W_S B_1 V$
$W_S B_1 V K_2$ 160
$W_S B_1 V K_2$ (70) 160
$W_S B_1 V K_2$ 140
$W_S B_1 V K_2$ (70) 140
$W_S B_1 V$
C_L
C_D
$C_{M_{a.c.}}$
α

Fig. 14

Fig. 15

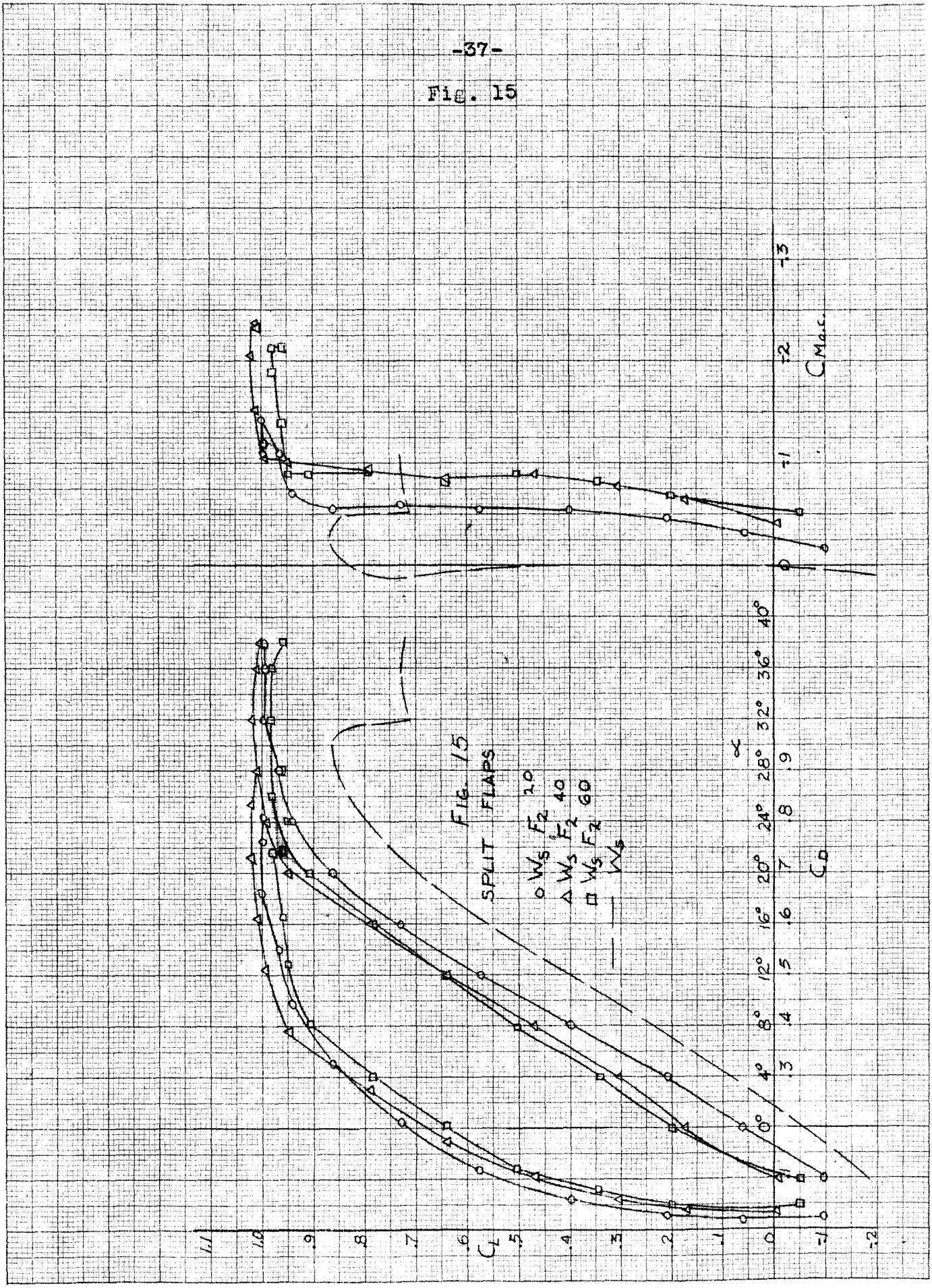
FIG. 15
SPLIT FLAPS
○ Ws F2 20
△ Ws F2 40
□ Ws F2 60
— Ws
CL
CD
CMac.
α
-4° 0° 4° 8° 12° 16° 20° 24° 28° 32° 36° 40°
-2 -1 0 1 2 3 4 5 6 7 8 9 10 11
-.2 -.1 0 .1 .2 .3 .4 .5 .6 .7 .8 .9
-.3 -.2 -.1 0 +.1 +.2

Fig. 16

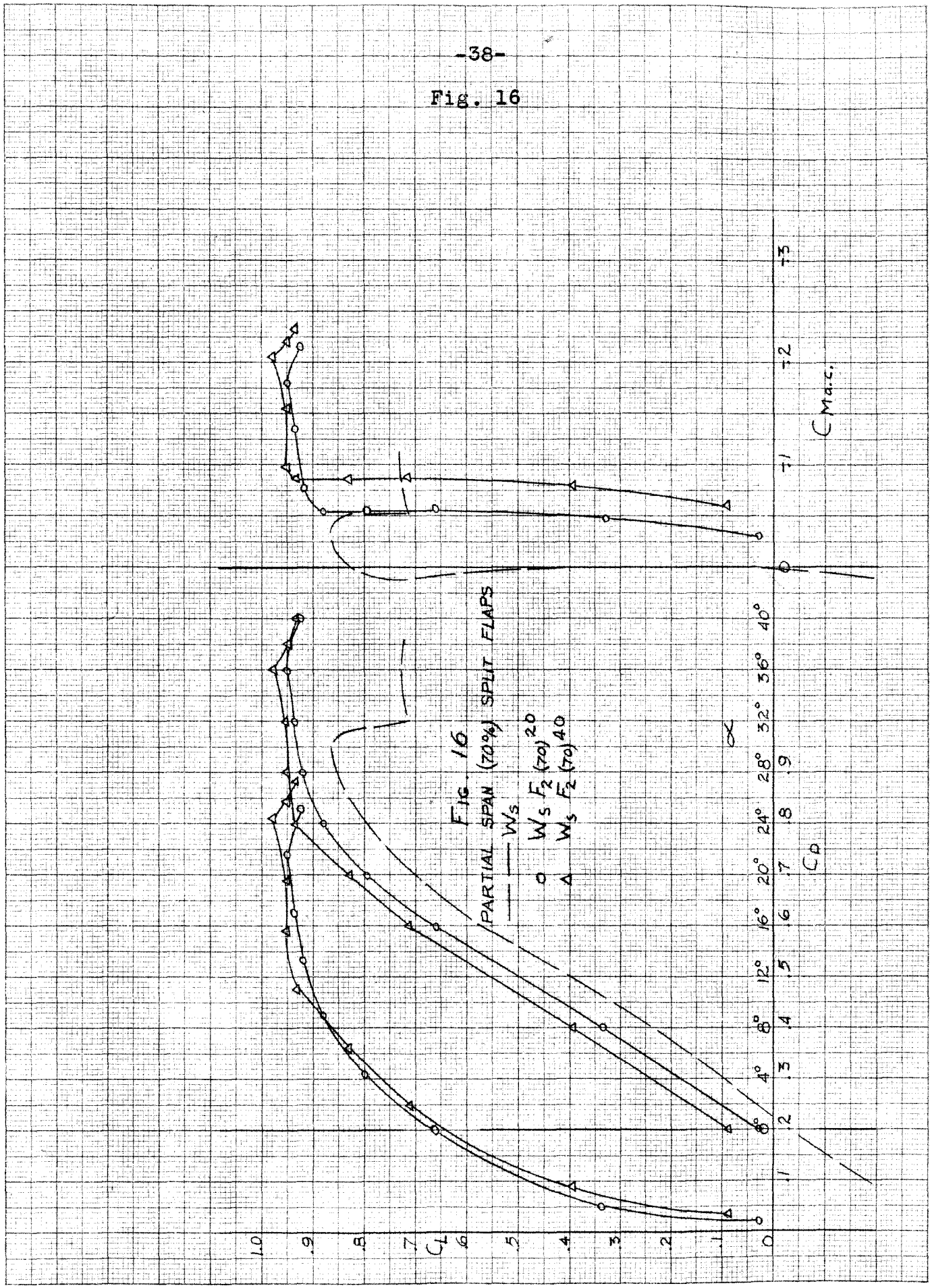
Fig. 16
PARTIAL SPAN (70%) SPLIT FLAPS
— — W_s
o W_s F_2 (70) 20
Δ W_s F_2 (70) 40
C_L
C_D
$C_{M.A.C.}$
α
1.0
.9
.8
.7
.6
.5
.4
.3
.2
.1
0
-.1
-.2
-.3
4°
8°
12°
16°
20°
24°
28°
32°
36°
40°
.1
.2
.3
.4
.5
.6
.7
.8
.9
-1
-2
-3

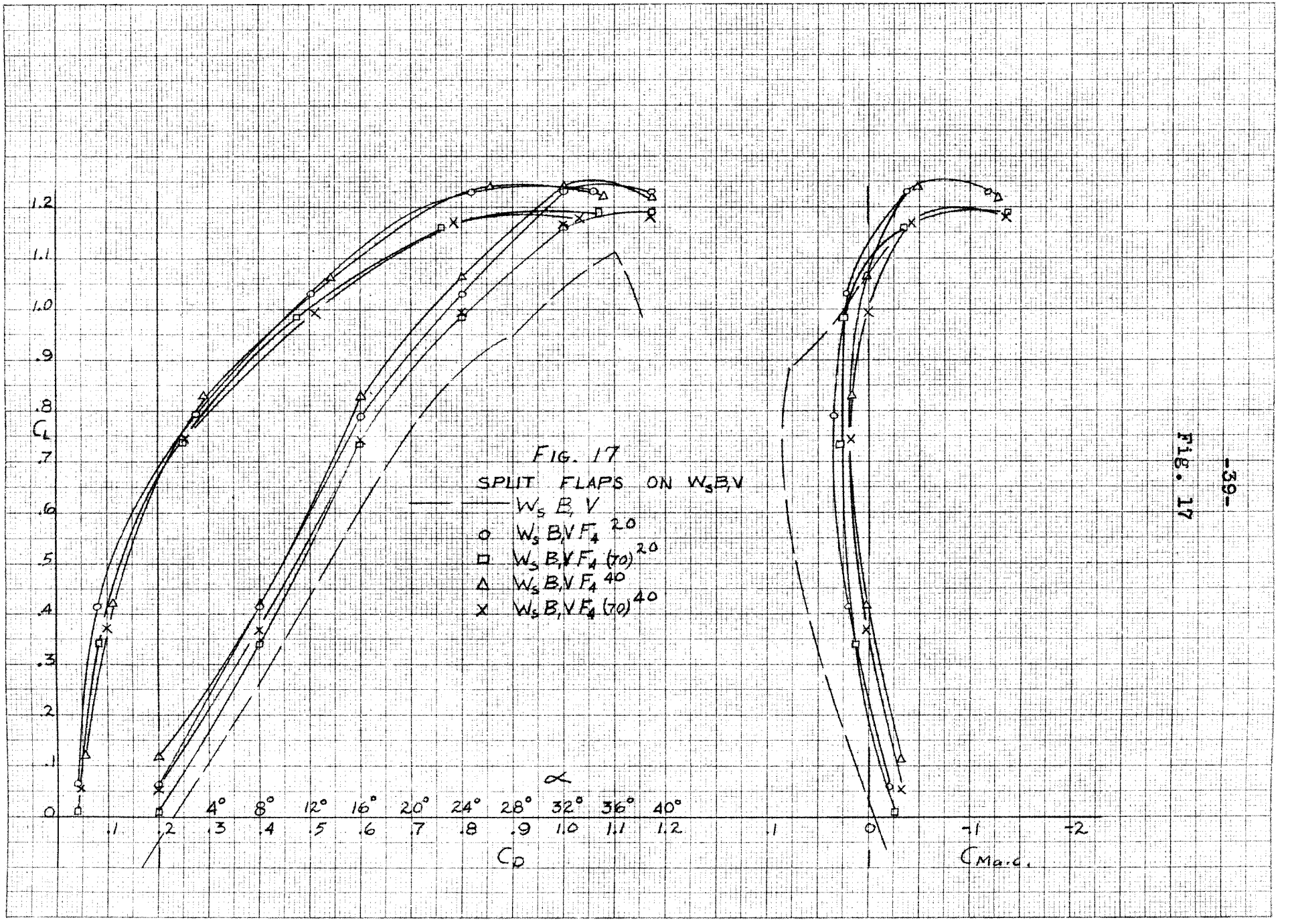

FIG. 17

SPLIT FLAPS ON $W_5 B_1 V$

Fig. 17

Fig. 18

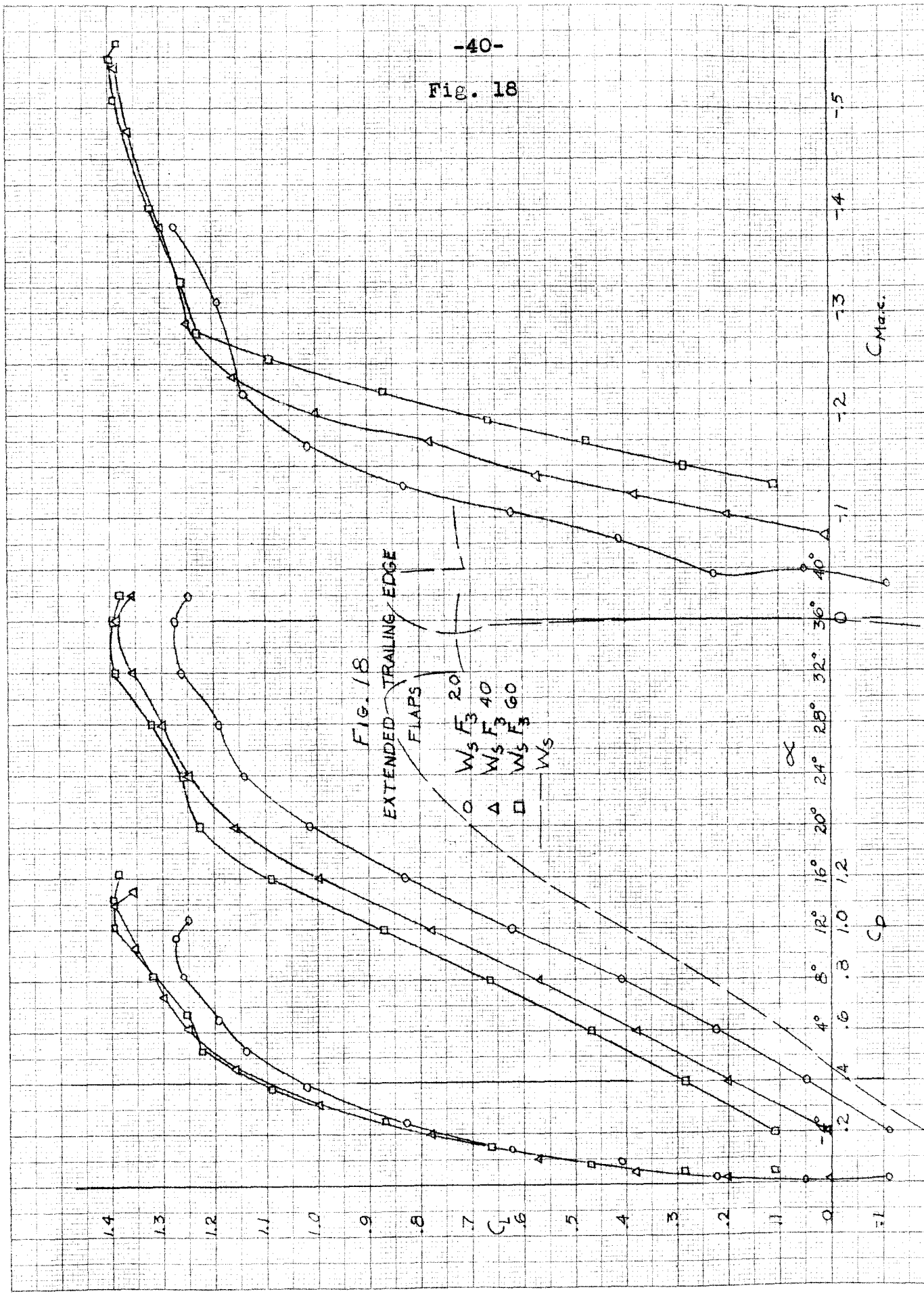
FIG. 18
EXTENDED TRAILING EDGE FLAPS
○ W_s F_3 20
△ W_s F_3 40
□ W_s F_3 60
— W_s
C_L
C_D
$C_{M.A.C.}$
α

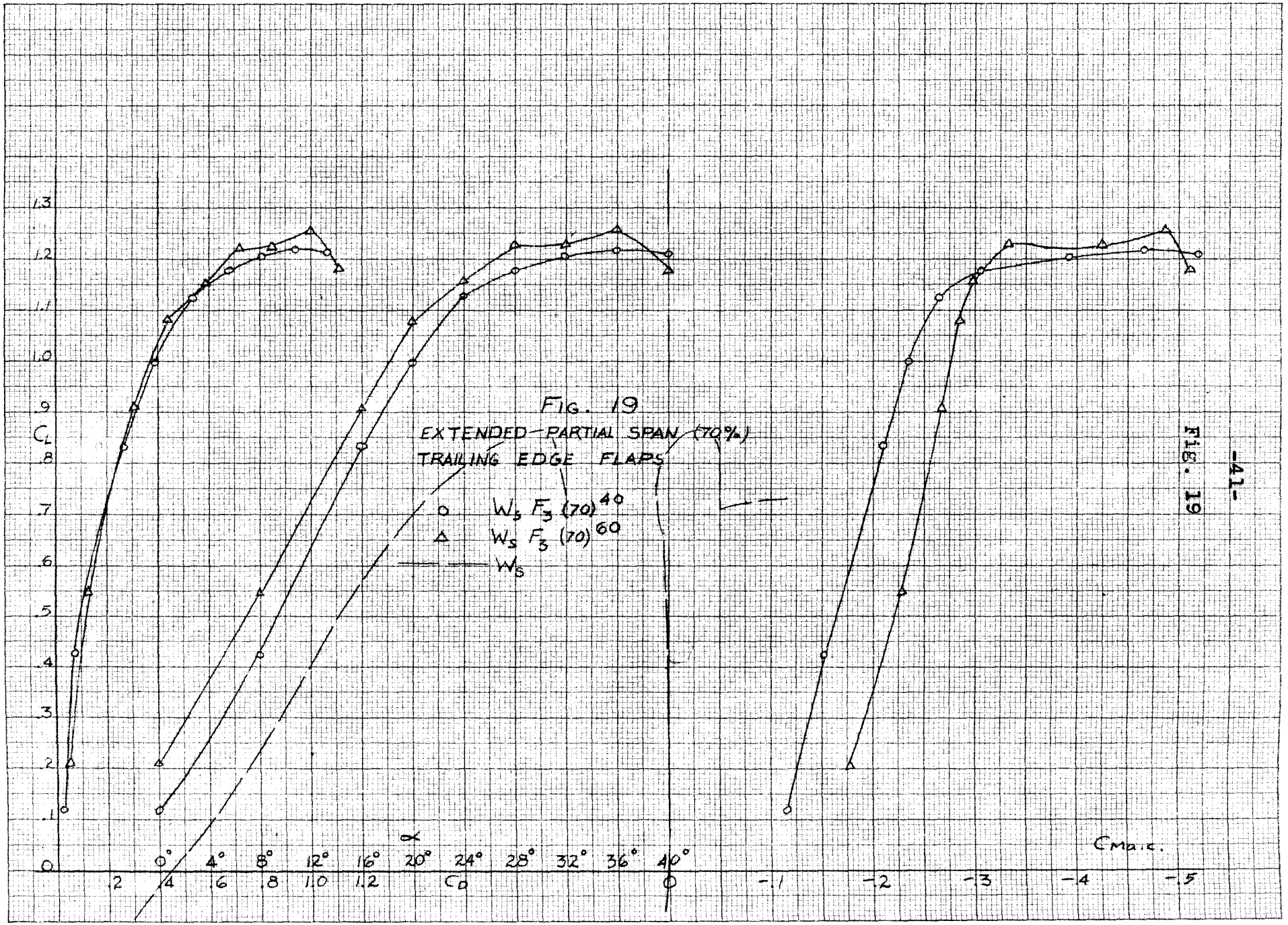
FIG. 19
EXTENDED—PARTIAL SPAN (70%)
TRAILING EDGE FLAPS
○ $W_5\ F_3\ (70)^{40}$
△ $W_5\ F_3\ (70)^{60}$
—— W_5
C_L
1.3
1.2
1.1
1.0
.9
.8
.7
.6
.5
.4
.3
.2
.1
0
α
0° 4° 8° 12° 16° 20° 24° 28° 32° 36° 40°
.2 .4 .6 .8 1.0 1.2
C_D
0
-.1 -.2 -.3 -.4 -.5
$C_{ma.c.}$

FIG. 19

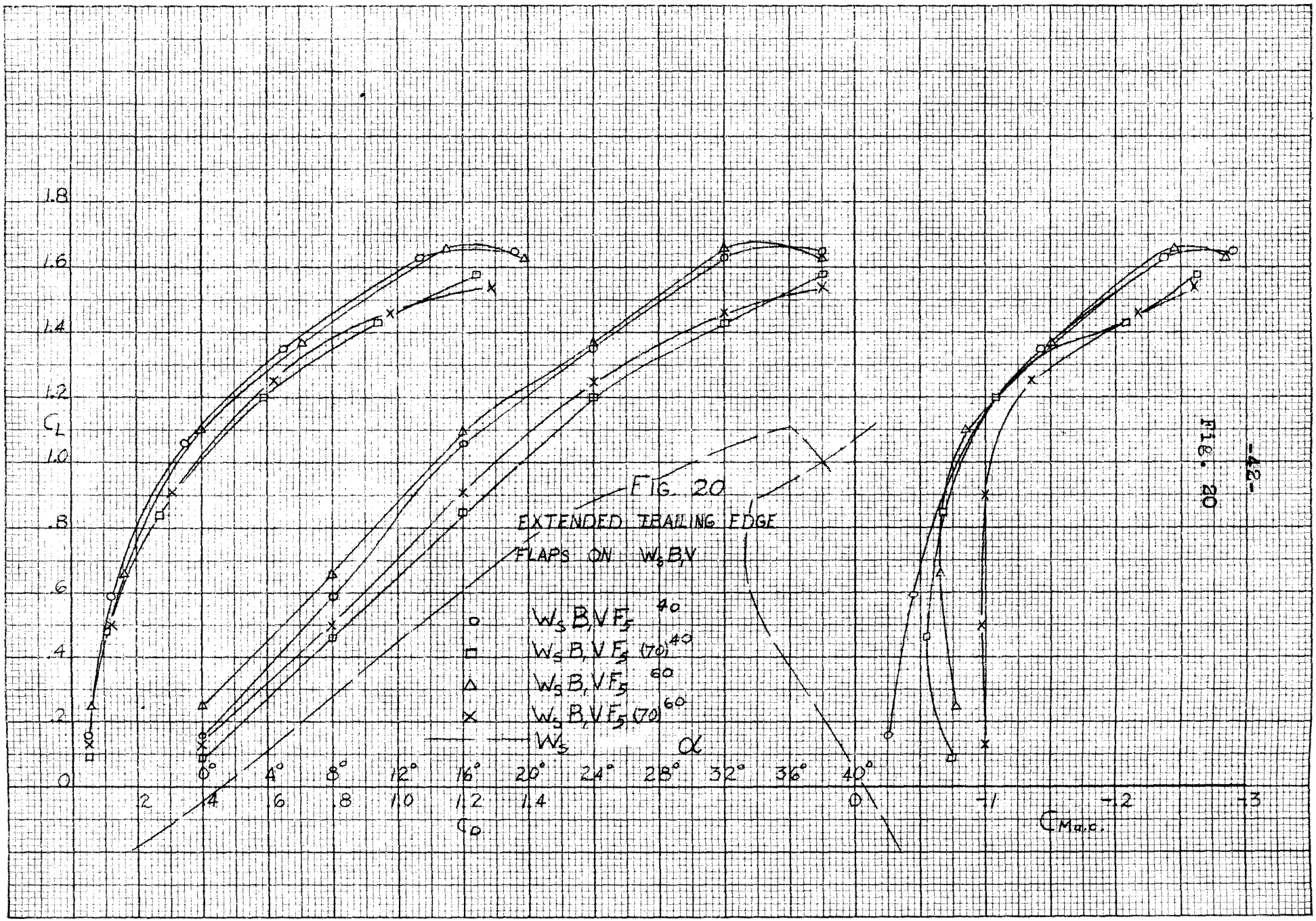
1.8
1.6
1.4
1.2
C_L
1.0
.8
.6
.4
.2
0
0°
4°
8°
12°
16°
20°
24°
28°
32°
36°
40°
α
.2
.4
.6
.8
1.0
1.2
1.4
C_D
0
-1
-2
-3
$C_{M_{a.c.}}$
EXTENDED TRAILING EDGE
FLAPS ON W_5B_1V
$W_5B_1VF_5$ 40
$W_5B_1VF_5$ (70) 40
$W_5B_1VF_5$ 60
$W_5B_1VF_5$ (70) 60
W_5

FIG. 20

FIG. 20

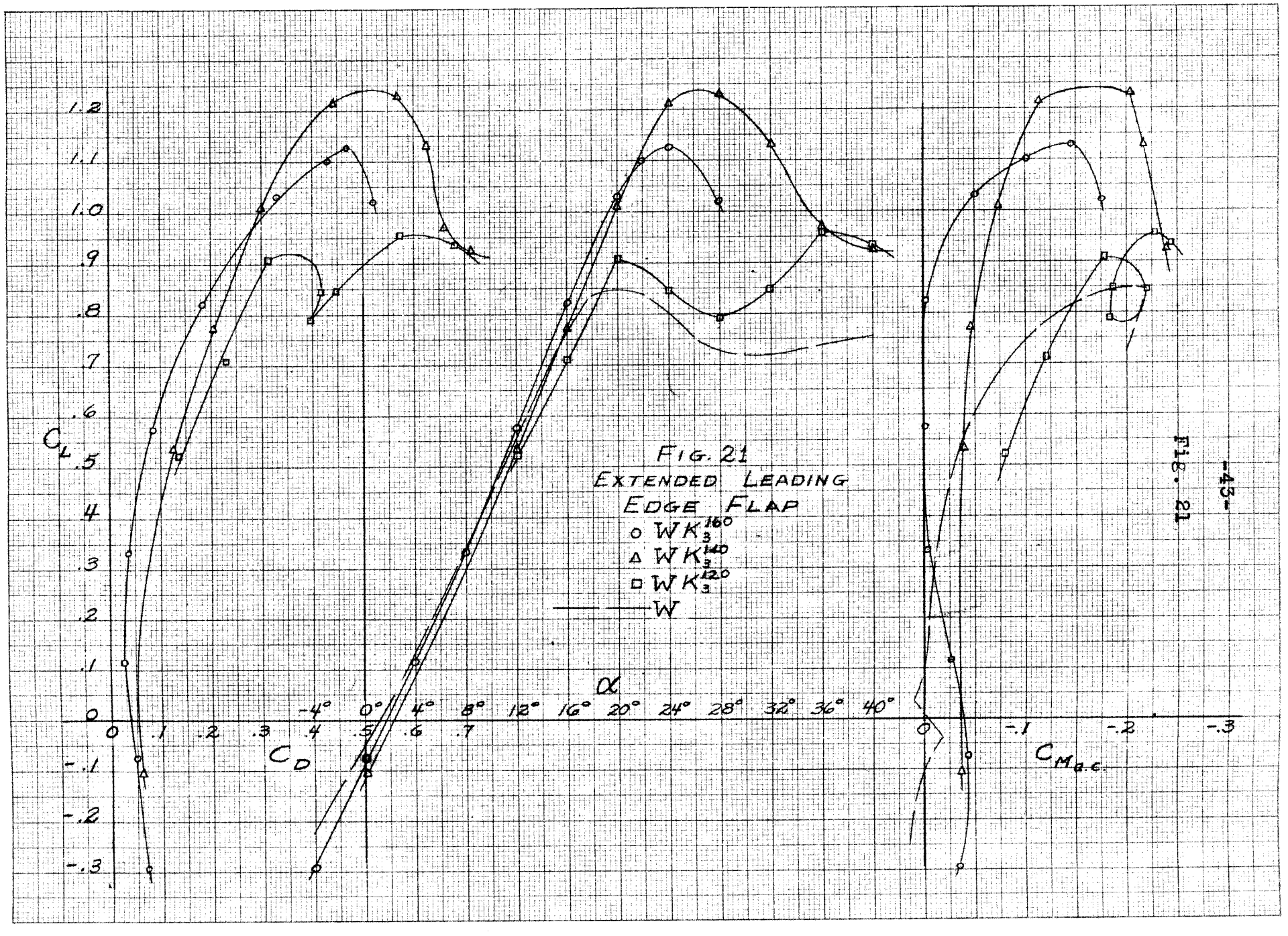
1.2
1.1
1.0
.9
.8
.7
.6
.5
.4
.3
.2
.1
0
C_L
-.1
-.2
-.3
-4°
0°
4°
8°
12°
16°
20°
24°
28°
32°
36°
40°
α
0
.1
.2
.3
.4
.5
.6
.7
C_D
0
-.1
-.2
-.3
$C_{M_{a.c.}}$
FIG. 21
EXTENDED LEADING
EDGE FLAP
○ WK_3^{160}
△ WK_3^{140}
□ WK_3^{120}
——— W

Fig. 21

Fig. 22

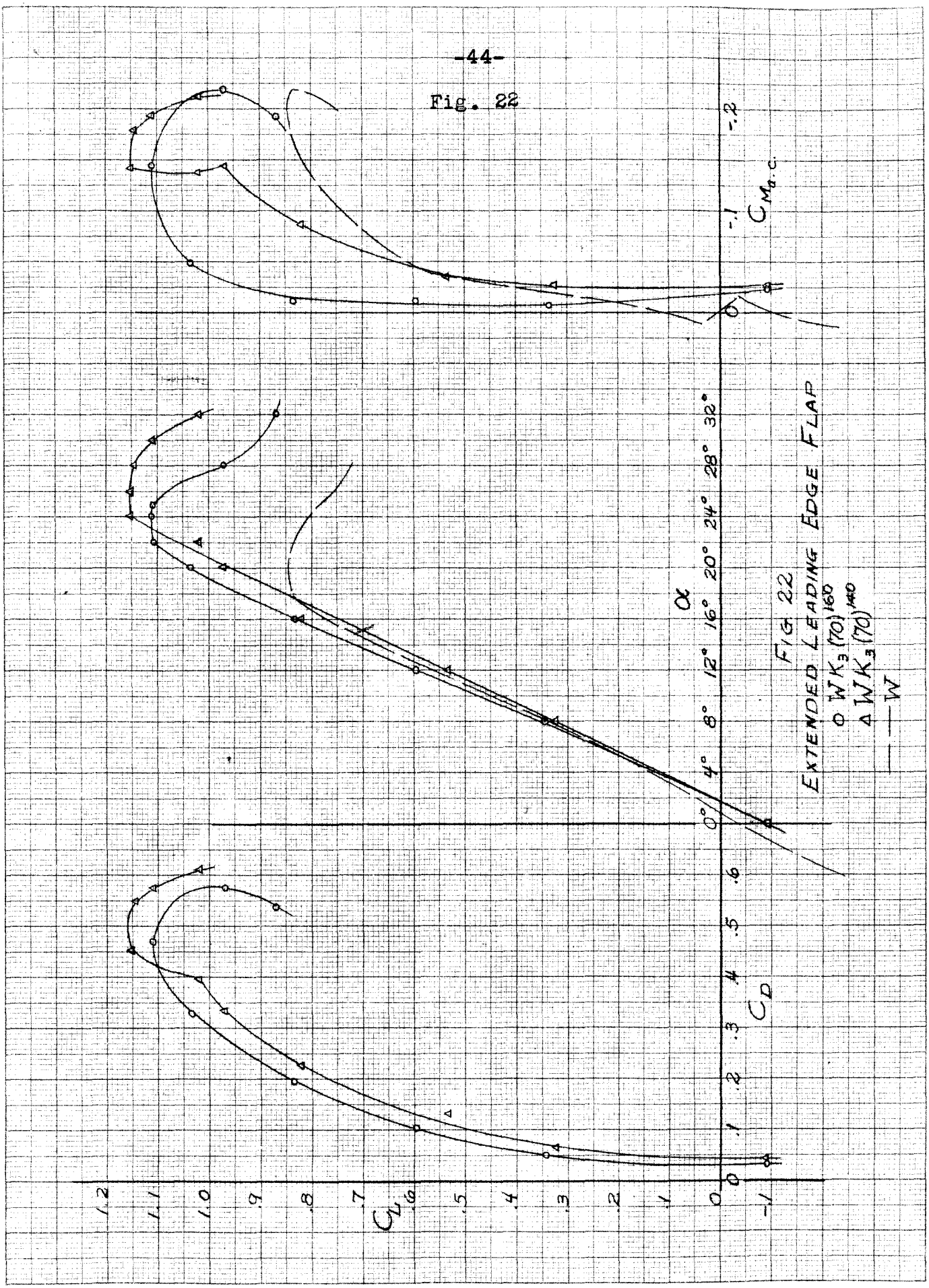
$C_{M_{a.c.}}$
-.2
-.1
C_D
C_L
α
0°
4°
8°
12°
16°
20°
24°
28°
32°
FIG 22
EXTENDED LEADING EDGE FLAP
○ WK_3 (70)^{160}
△ WK_3 (70)^{140}
—— W

Fig. 23

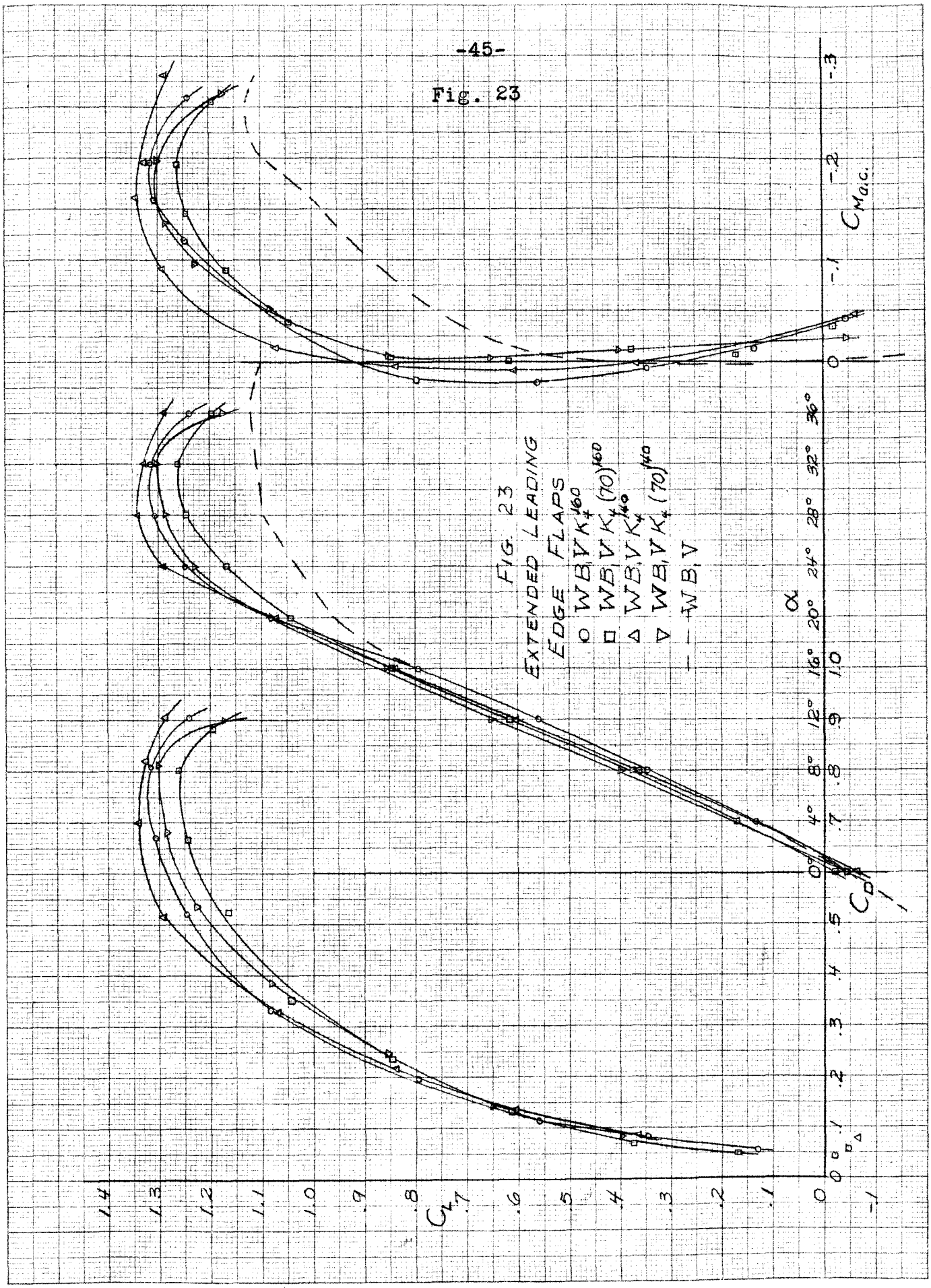
FIG. 23
EXTENDED LEADING EDGE FLAPS
○ WBV K_4^{160}
□ WBV K_4^{160} (70)
△ WBV K_4^{140}
▽ WBV K_4^{140} (70)
— — WBV
α
0° 4° 8° 12° 16° 20° 24° 28° 32° 36°
C_L
C_D
$C_{M.C.}$

Fig. 24

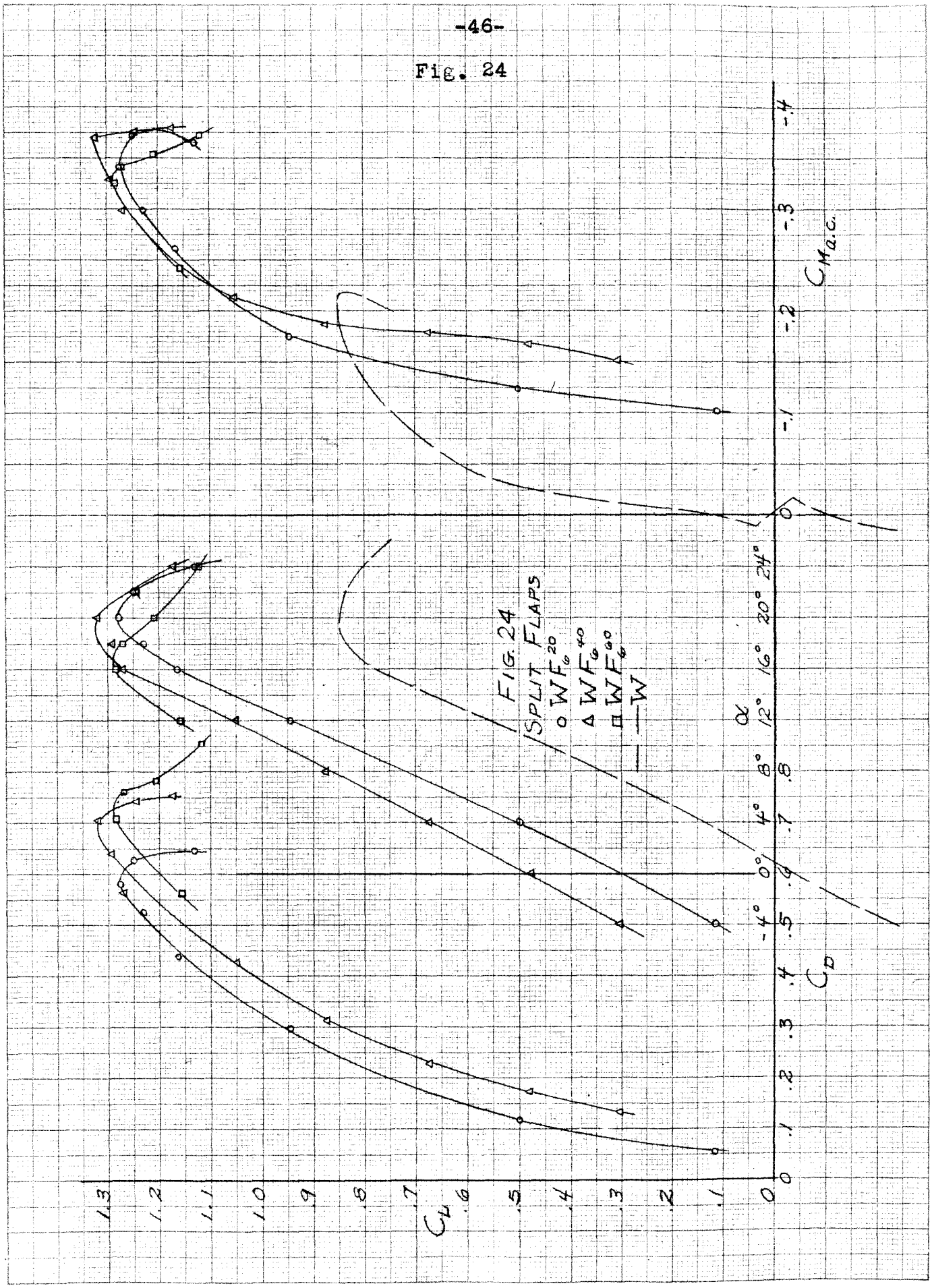
FIG. 24
SPLIT FLAPS
○ WF 20
△ WF 40
□ WF 60
— W
α
-4° 0° 4° 8° 12° 16° 20° 24°
C_L
0 .1 .2 .3 .4 .5 .6 .7 .8 .9 1.0 1.1 1.2 1.3
C_D
0 .1 .2 .3 .4 .5 .6 .7 .8
$C_{M_{a.c.}}$
0 -.1 -.2 -.3 -.4

Fig. 25

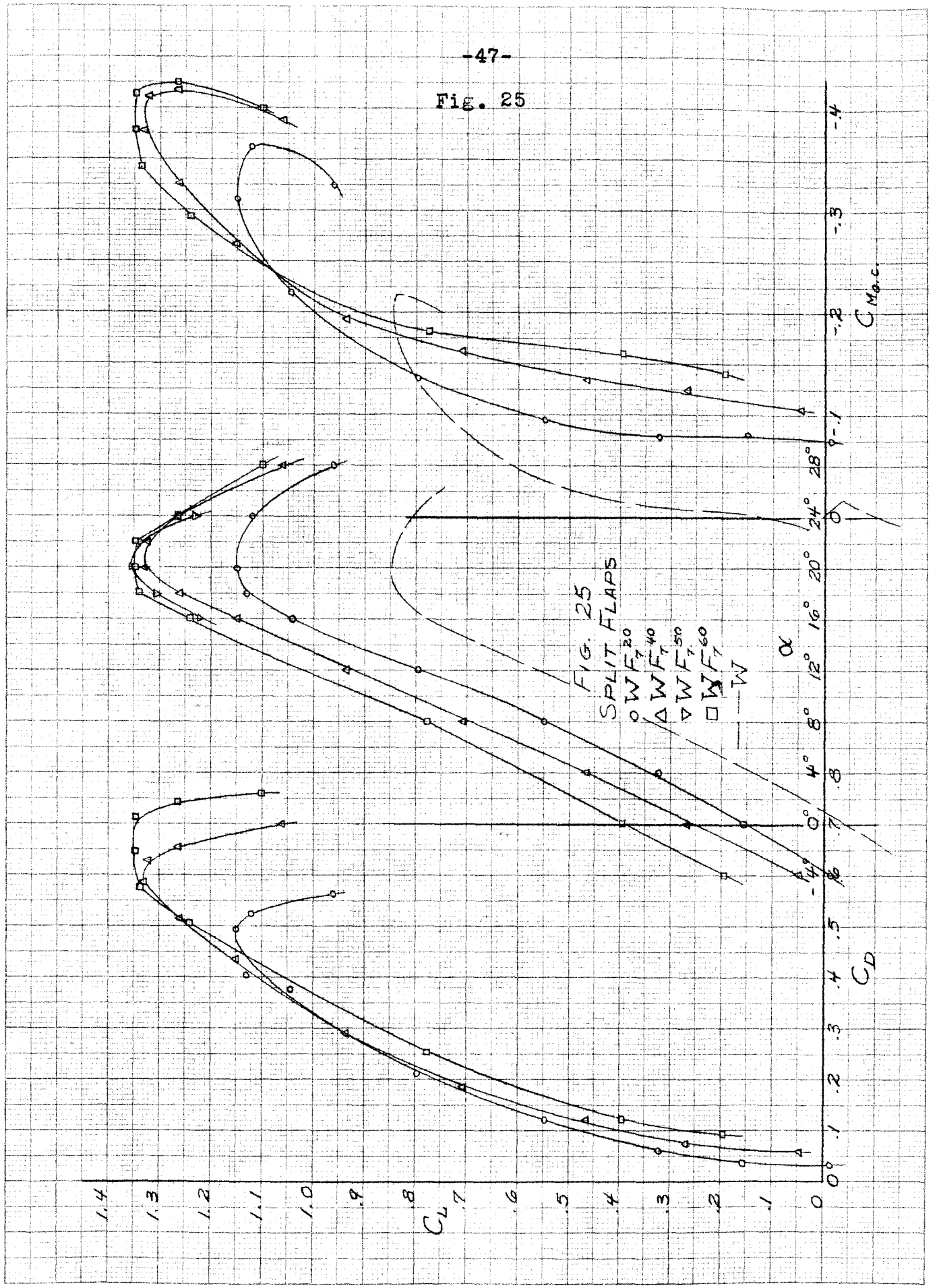

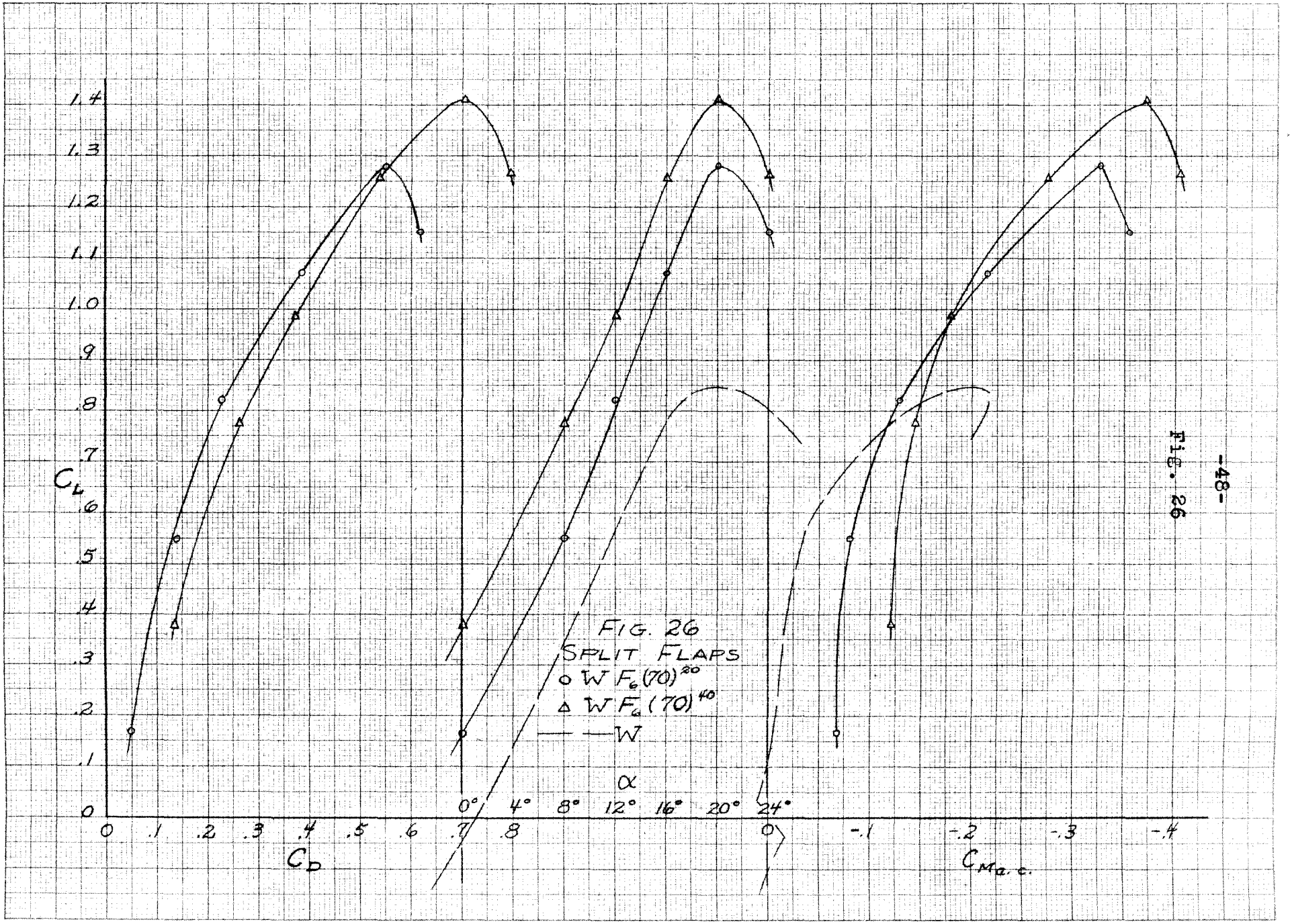
1.4
1.3
1.2
1.1
1.0
.9
.8
.7
.6
.5
.4
.3
.2
.1
0
C_L
0 .1 .2 .3 .4 .5 .6 .7 .8
C_D
0
-.1 -.2 -.3 -.4
$C_{M_{a.c.}}$
FIG. 26
SPLIT FLAPS
o W $F_6(70)^{20}$
Δ W $F_6(70)^{40}$
— — W
α
0° 4° 8° 12° 16° 20° 24°

Fig. 26

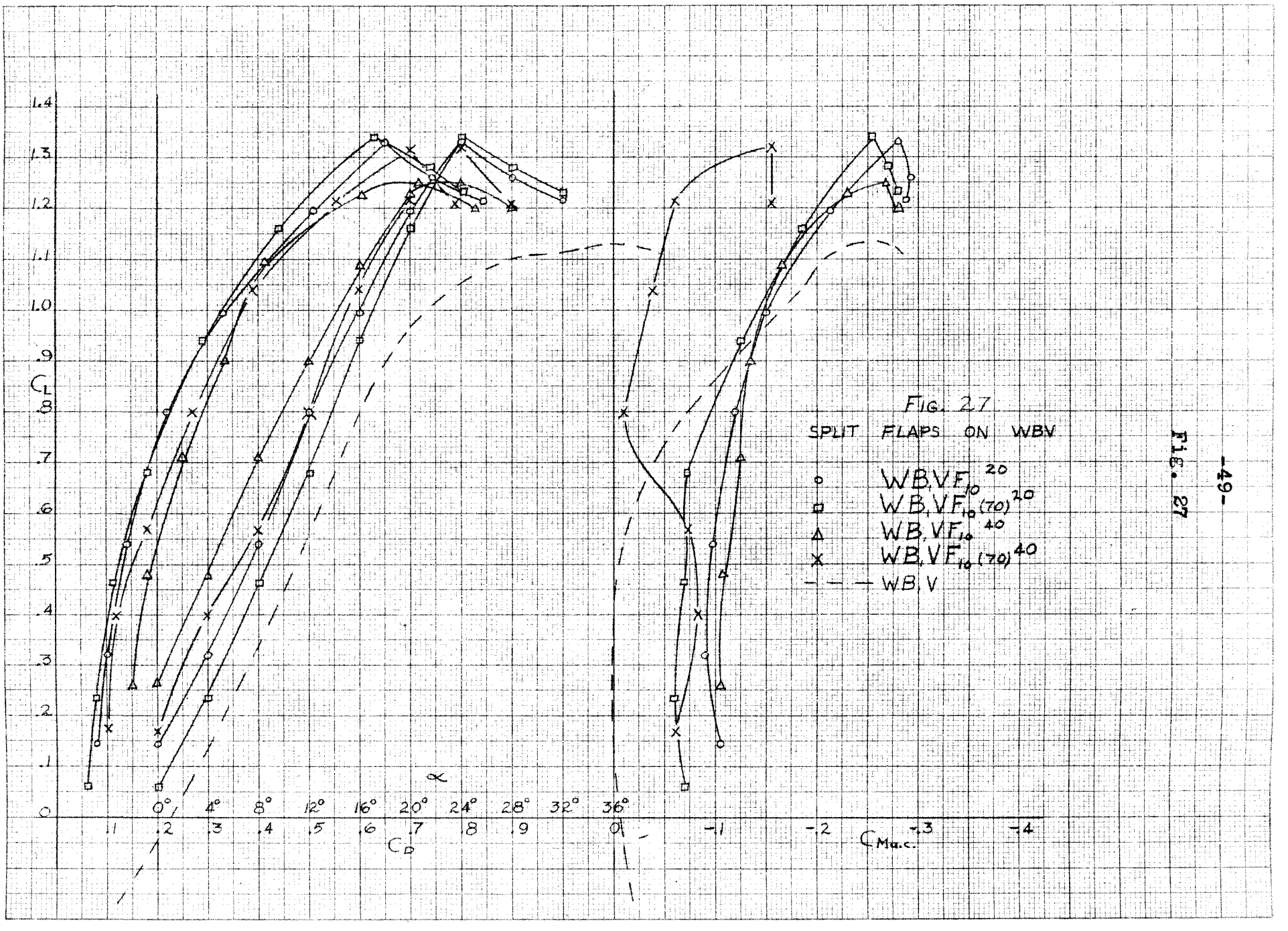

FIG. 27

SPLIT FLAPS ON WBV

FIG. 27

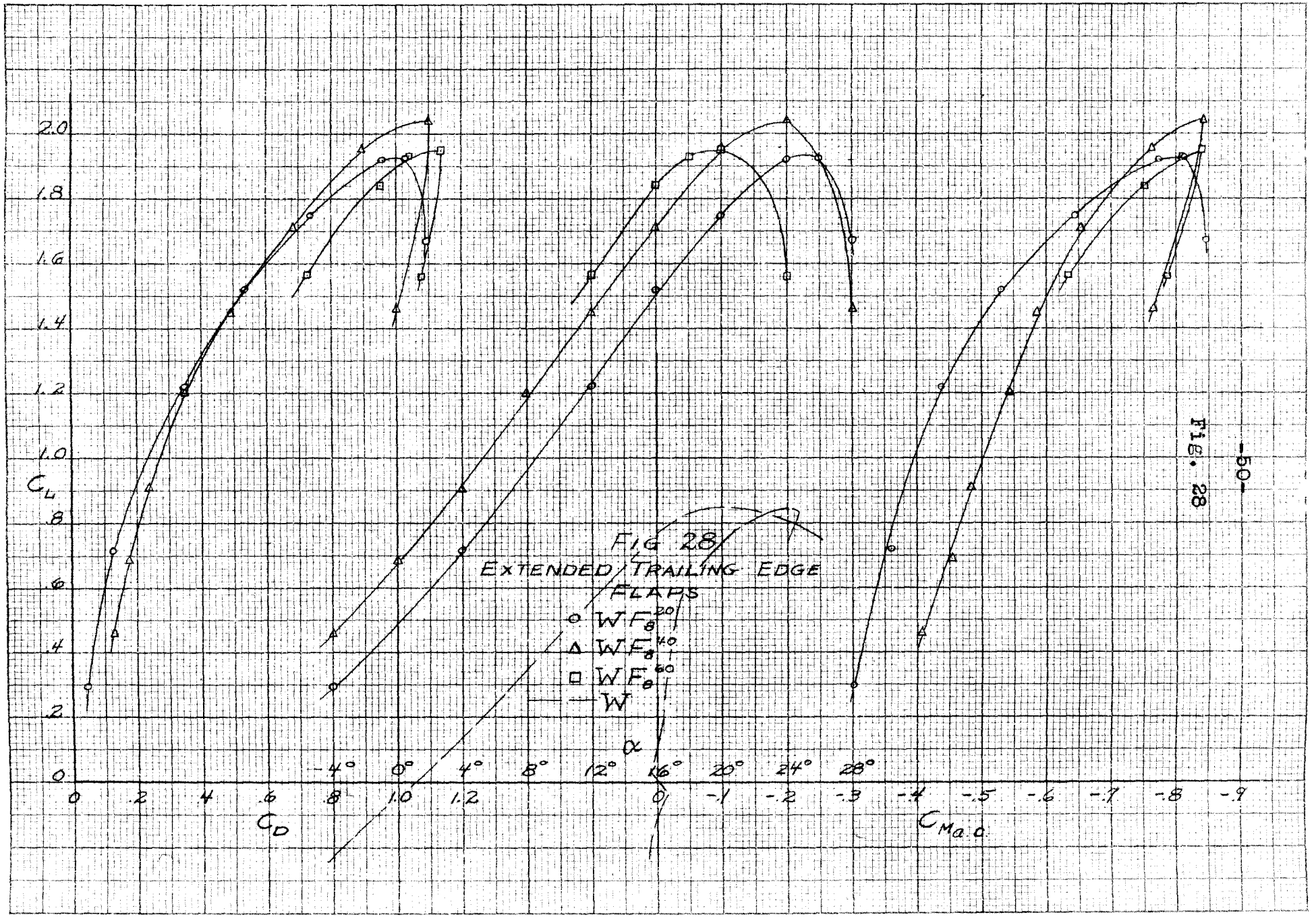
2.0
1.8
1.6
1.4
1.2
1.0
C_L
.8
.6
.4
.2
0
-4°
0°
4°
8°
12°
16°
20°
24°
28°
α
0
.2
.4
.6
.8
1.0
1.2
C_D
0
-.1
-.2
-.3
-.4
-.5
-.6
-.7
-.8
-.9
$C_{Ma.c}$
FIG 28
EXTENDED TRAILING EDGE
FLAPS
○ WF_{δ}^{20}
△ WF_{δ}^{40}
□ WF_{δ}^{60}
— W

Fig. 28

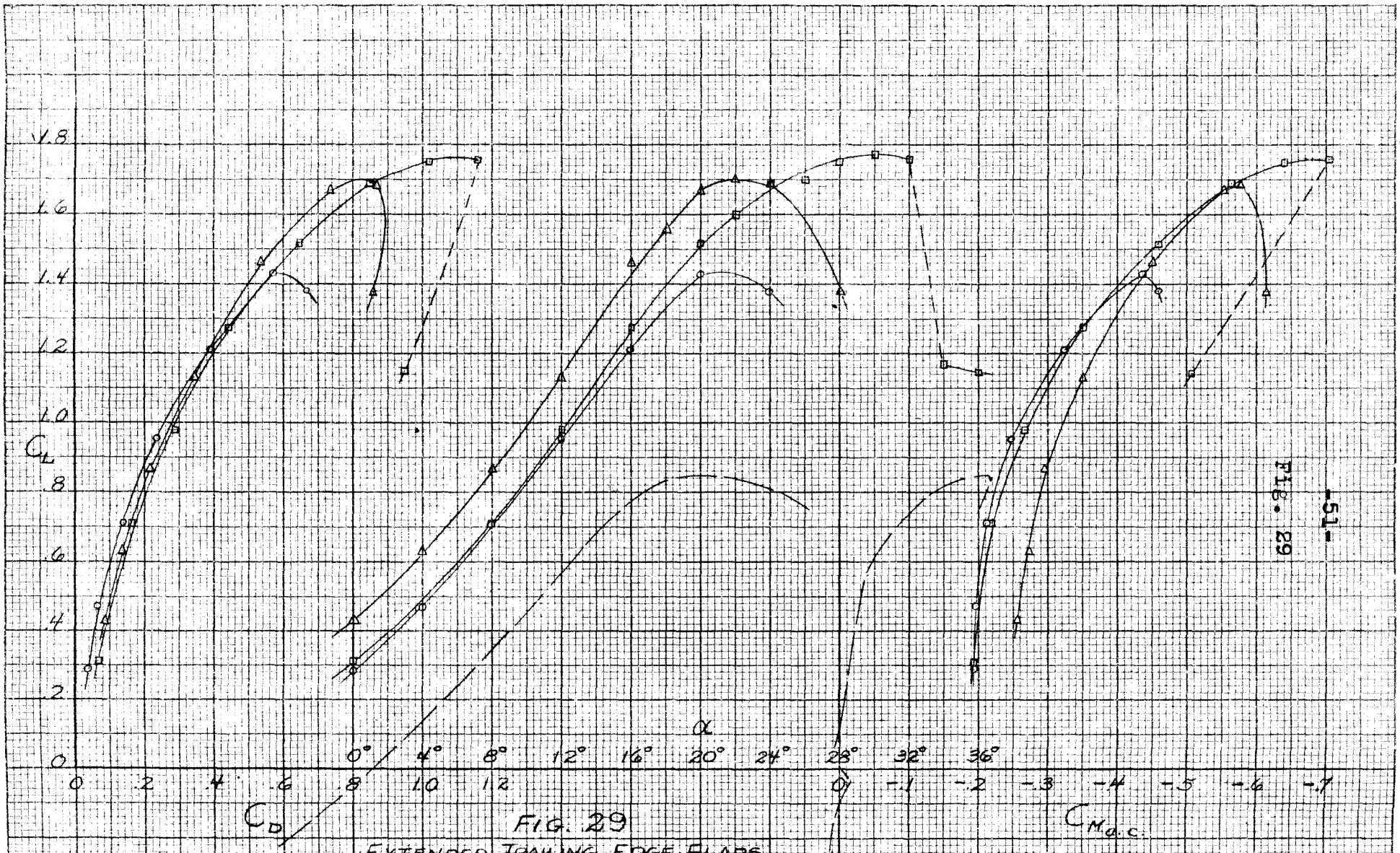

FIG. 29

EXTENDED TRAILING EDGE FLAPS

- o WF_9^{20}
- △ WF_9^{40}
- □ $WF_9(70)^{40}$
- —— W

Fig. 29

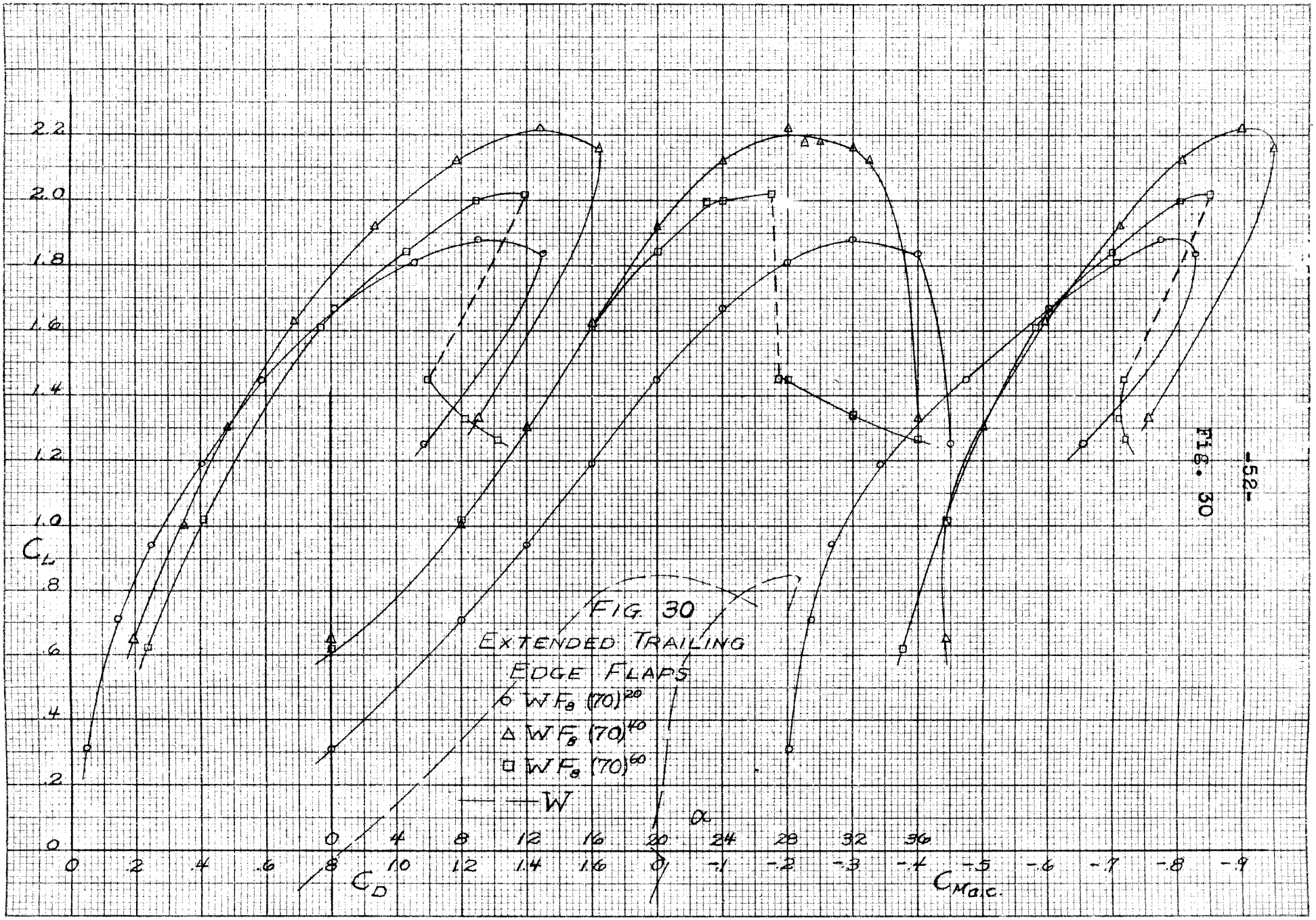
2.2
2.0
1.8
1.6
1.4
1.2
1.0
.8
.6
.4
.2
0
C_L
0 .2 .4 .6 .8 1.0 1.2 1.4 1.6
C_D
0 4 8 12 16 20 24 28 32 36
α
0 -1 -2 -3 -4 -5 -6 -7 -8 -9
$C_{M a.c.}$
FIG. 30
EXTENDED TRAILING
EDGE FLAPS
○ WF_8 $(70)^{20}$
△ WF_8 $(70)^{40}$
□ WF_8 $(70)^{60}$
— — W

Fig. 30

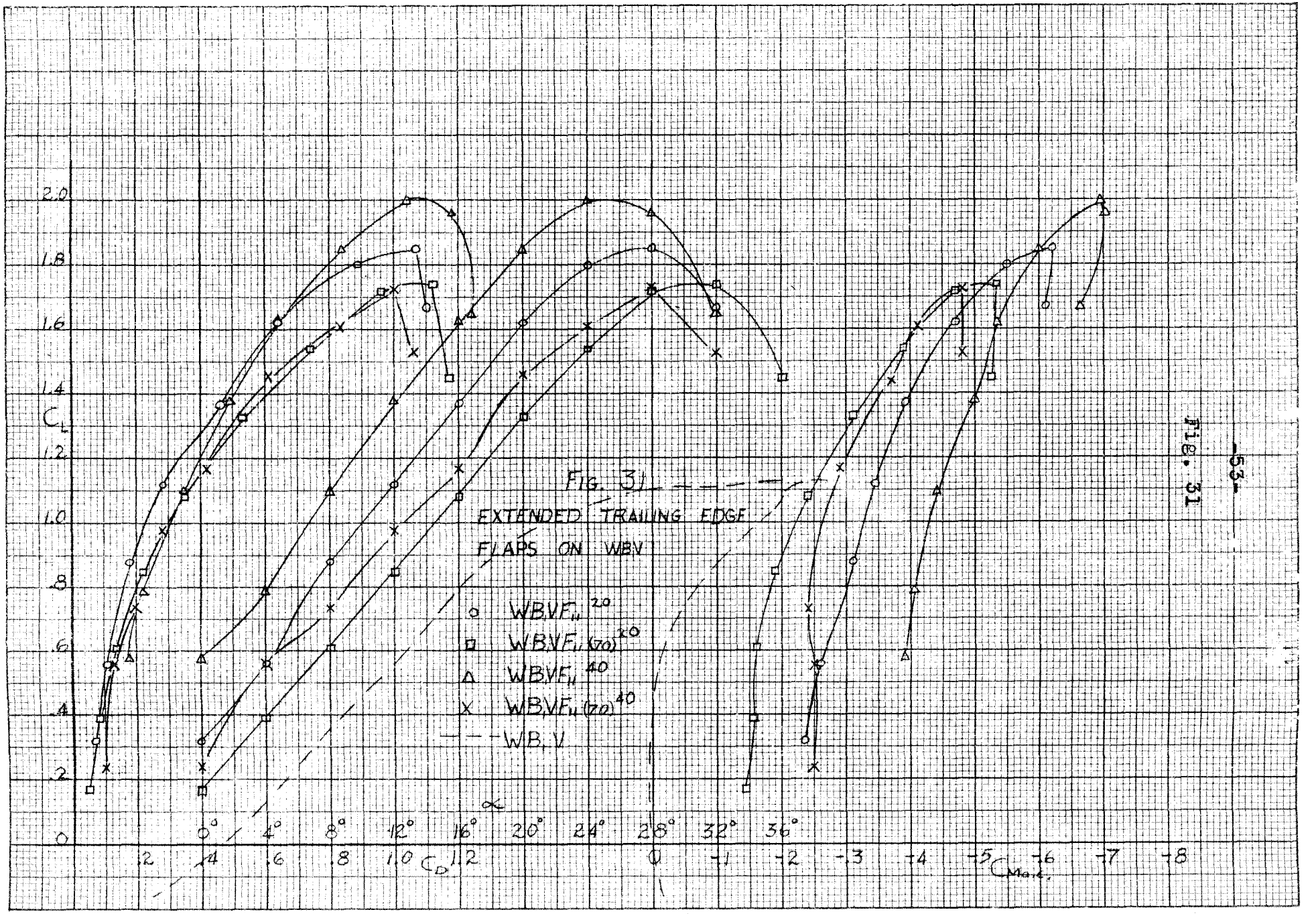
FIG. 31
EXTENDED TRAILING EDGE FLAPS ON WBV
WBVF$_{11}^{20}$
WBVF$_{11(70)}^{20}$
WBVF$_{11}^{40}$
WBVF$_{11(70)}^{40}$
WB,V
C_L
C_D
$C_{M_{a.c.}}$
α
2.0
1.8
1.6
1.4
1.2
1.0
.8
.6
.4
.2
0
0°
4°
8°
12°
16°
20°
24°
28°
32°
36°
.2
.4
.6
.8
1.0
1.2
0
-1
-2
-3
-4
-5
-6
-7
-8

FIG. 32 $C_{L\,MAX.}$ vs. FLAP DEFLECTION

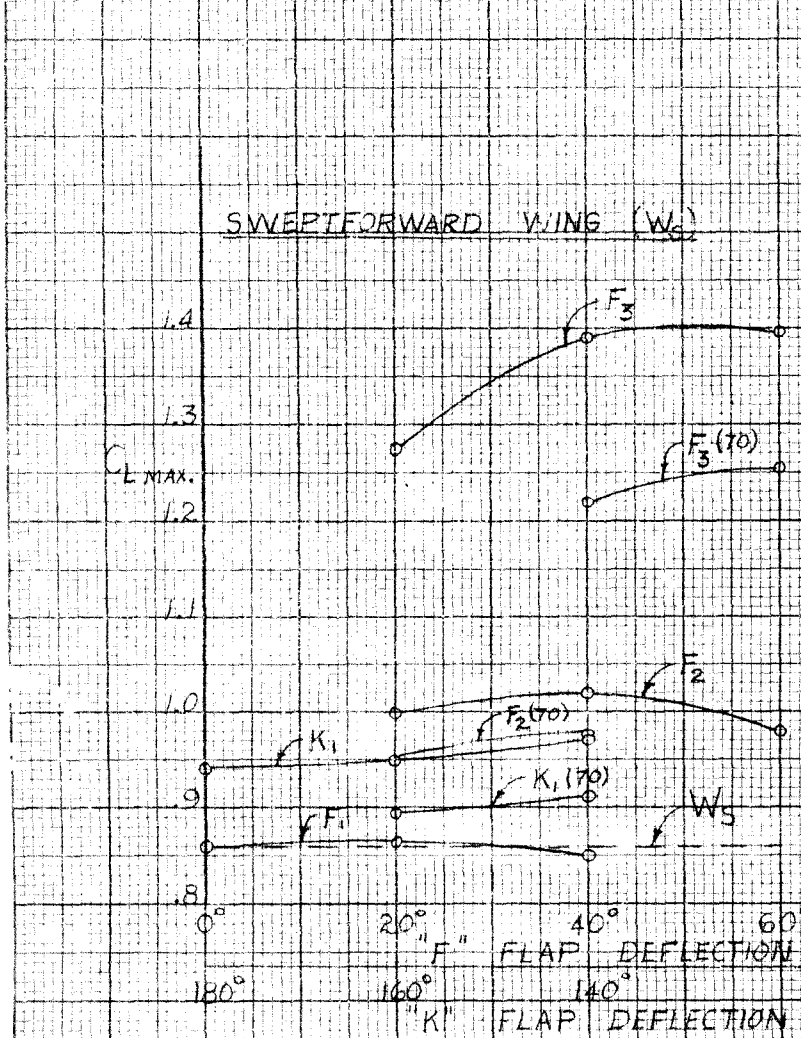

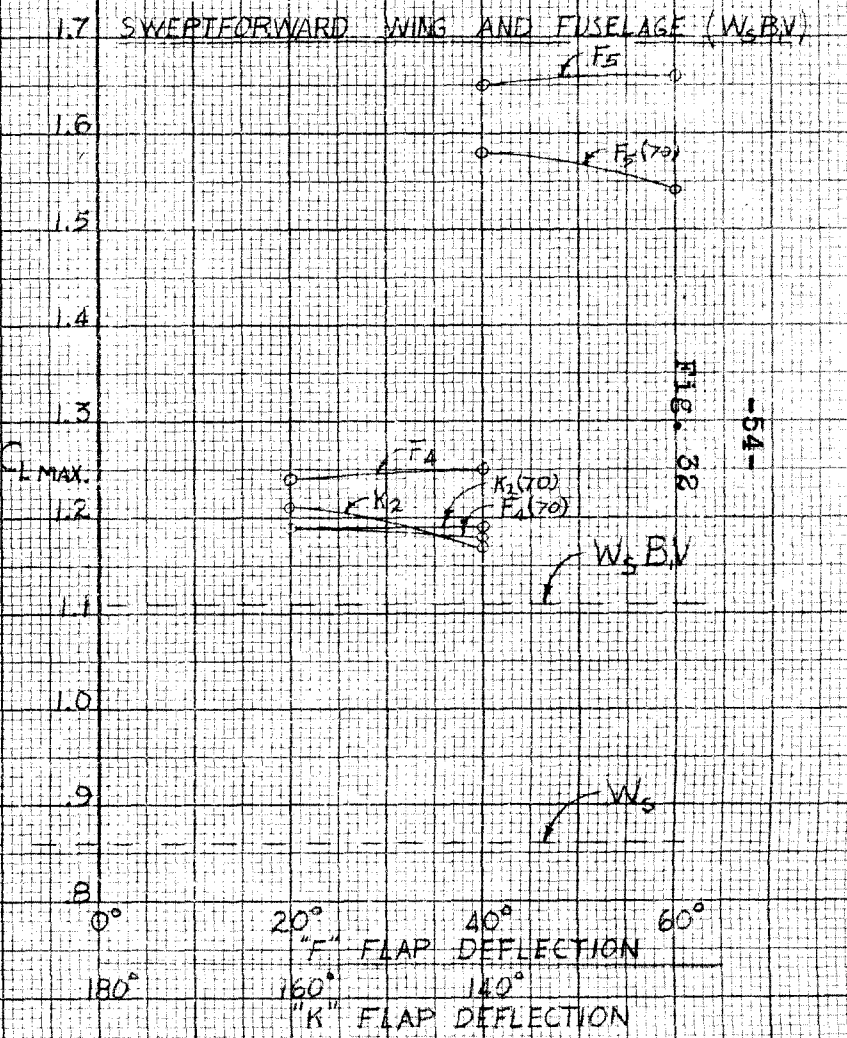

FIG. 32

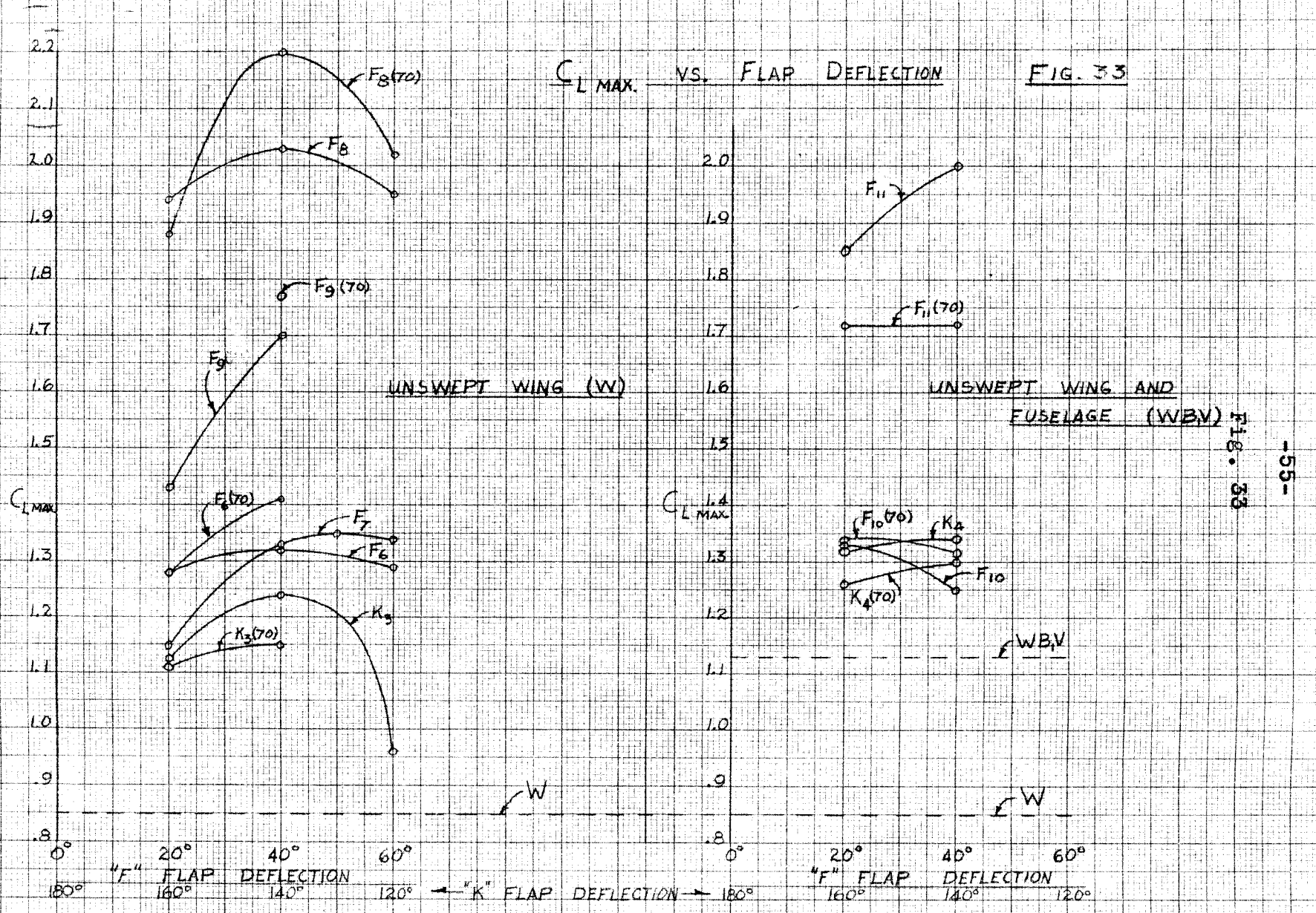
$C_{L\ MAX.}$ VS. FLAP DEFLECTION
FIG. 33
UNSWEPT WING (W)
UNSWEPT WING AND FUSELAGE (WB1V)
$C_{L\ MAX.}$
2.2
2.1
2.0
1.9
1.8
1.7
1.6
1.5
1.4
1.3
1.2
1.1
1.0
.9
.8
$F_8(70)$
F_8
$F_9(70)$
F_9
$F_5(70)$
F_7
F_6
K_3
$K_3(70)$
W
F_{11}
$F_{11}(70)$
$F_{10}(70)$
K_4
F_{10}
$K_4(70)$
WB_1V
0°
20°
40°
60°
"F" FLAP DEFLECTION
180°
160°
140°
120°
"K" FLAP DEFLECTION

Fig. 33

Fig. 34

W

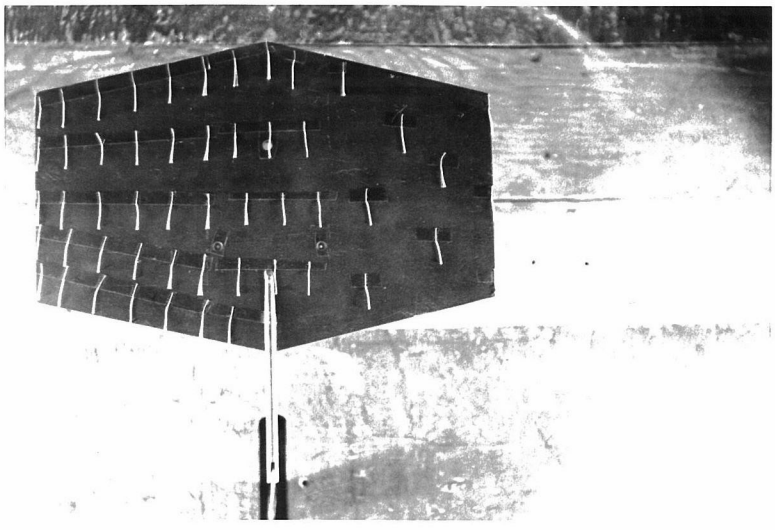

$\alpha = 0°$

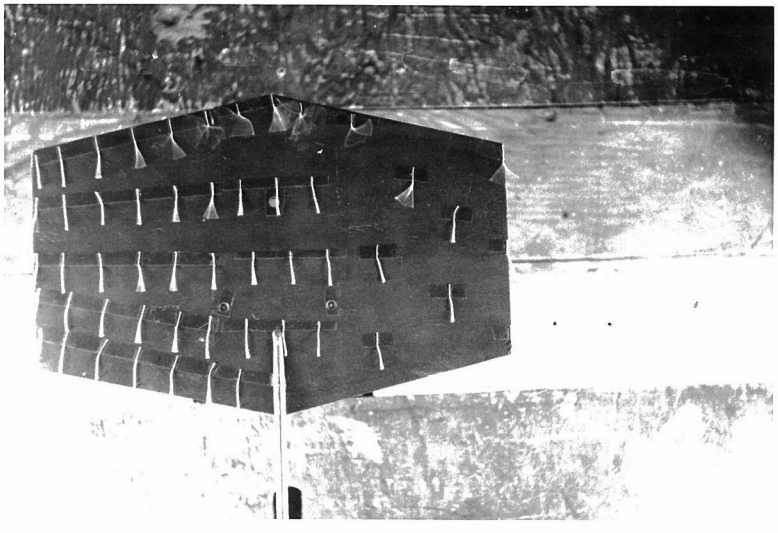

$\alpha = 5°$

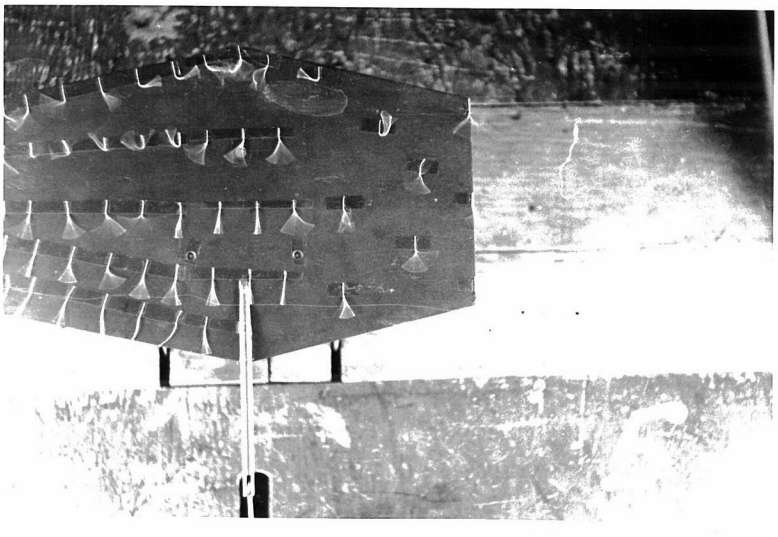

$\alpha = 12°$

Fig. 35

W

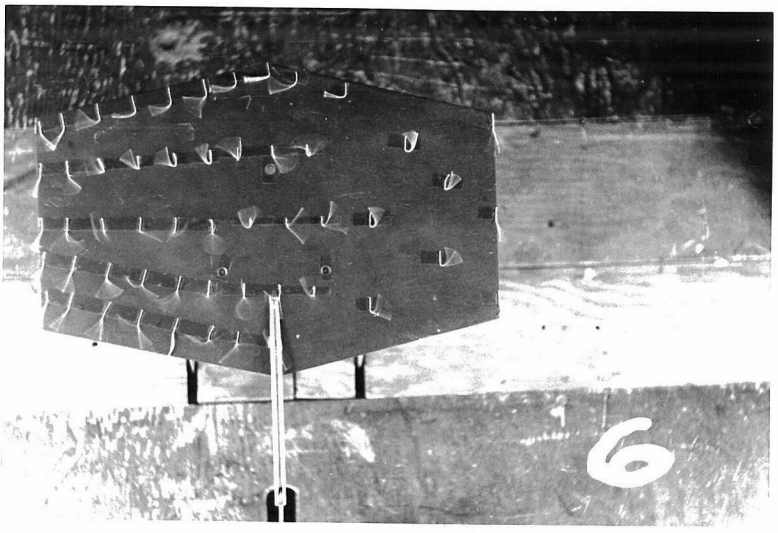

$\alpha = 15°$

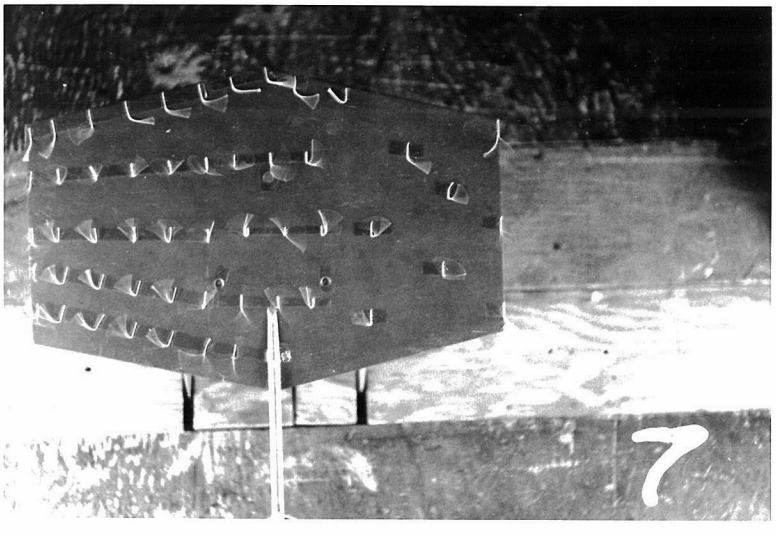

$\alpha = 20°$

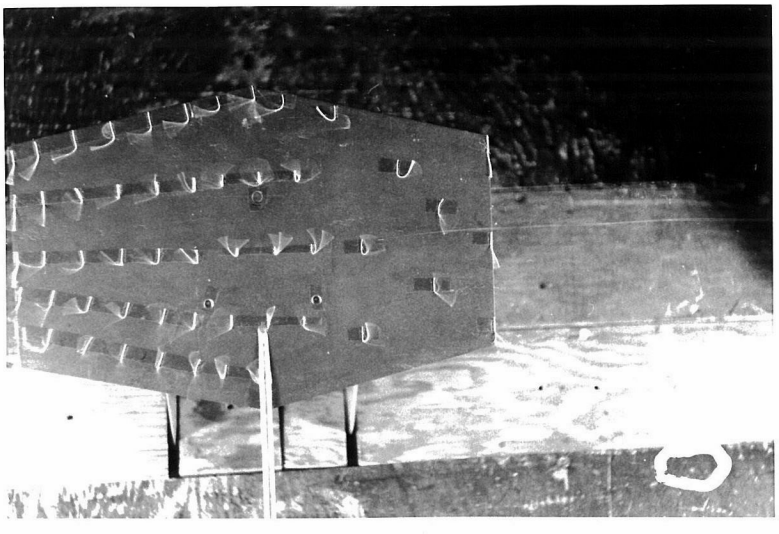

$\alpha = 28°$

Fig. 36

WB_1V

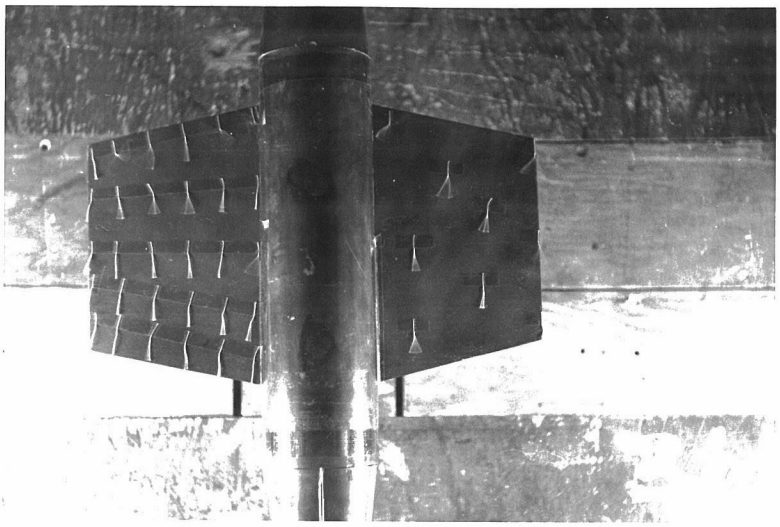

$\alpha = 8°$

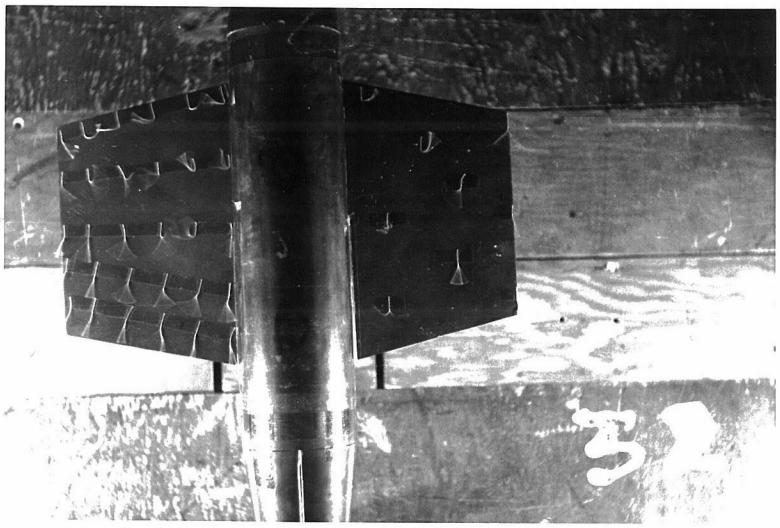

$\alpha = 10°$

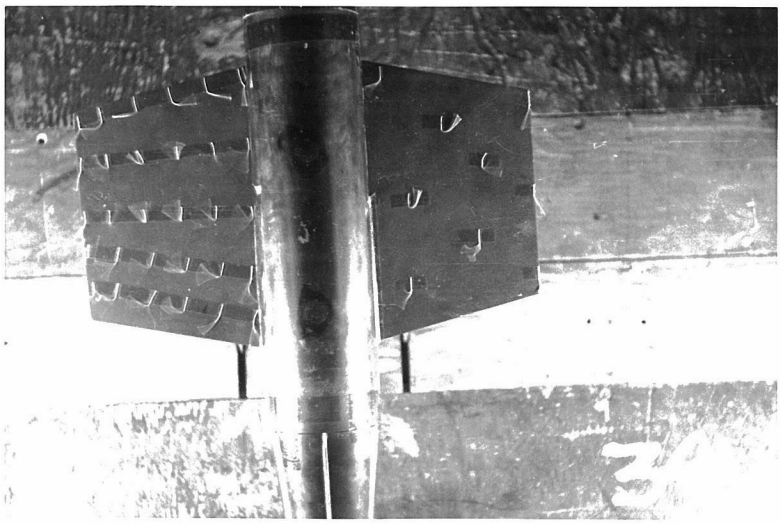

$\alpha = 18°$

Fig. 37

WB_1V

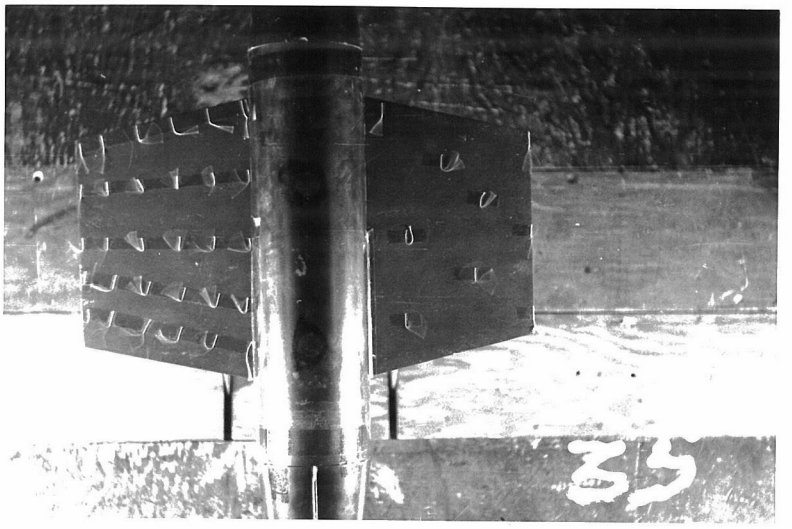

$\alpha = 20^\circ$

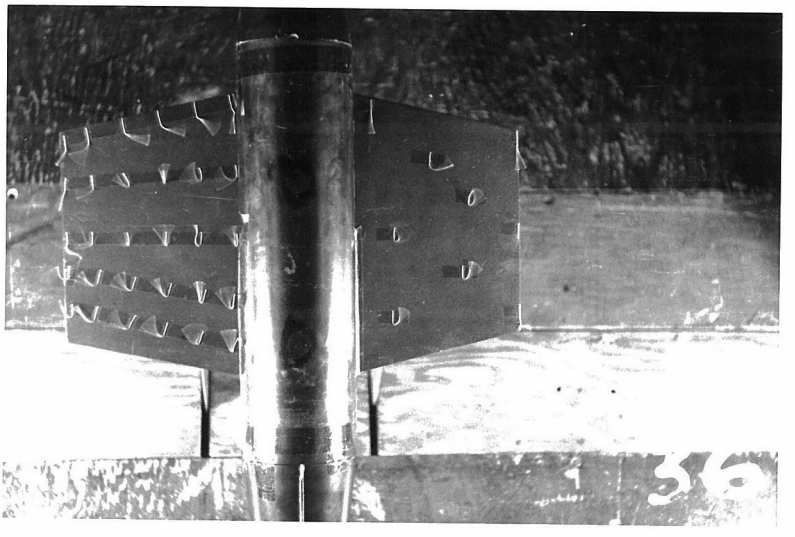

$\alpha = 26^\circ$

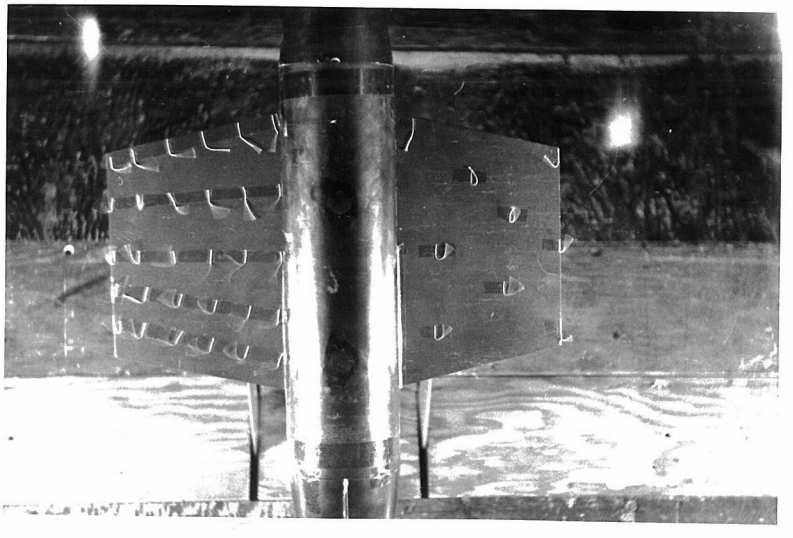

$\alpha = 36^\circ$

Fig. 38

W_s

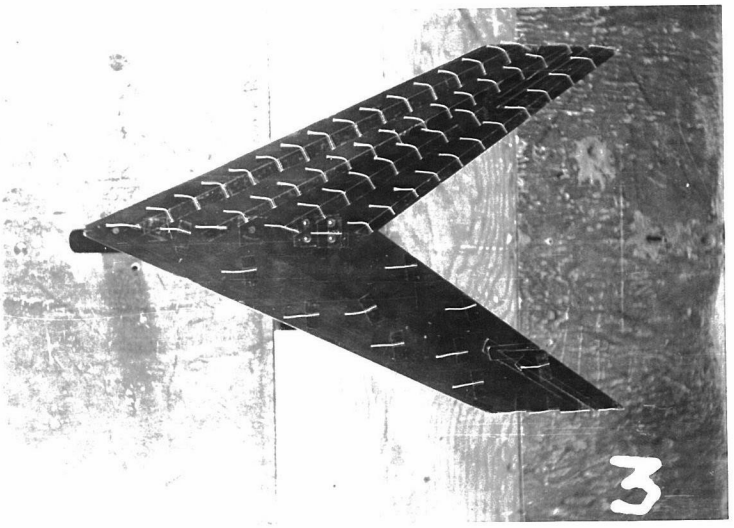

$\alpha = 0°$

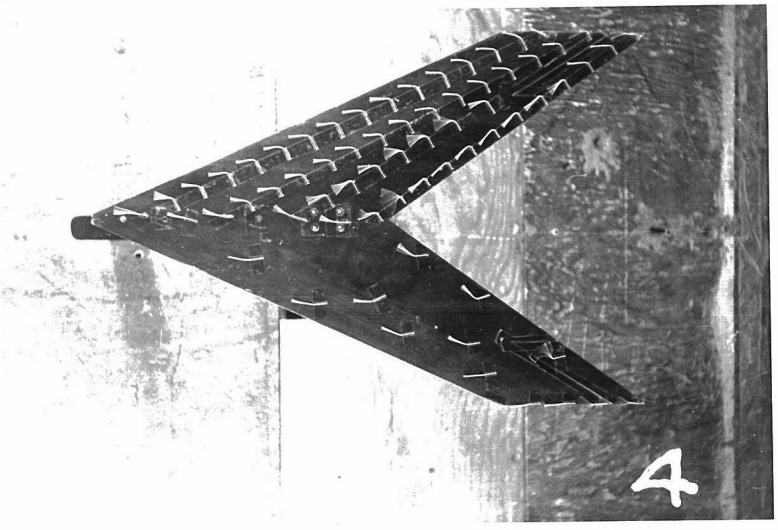

$\alpha = 8°$

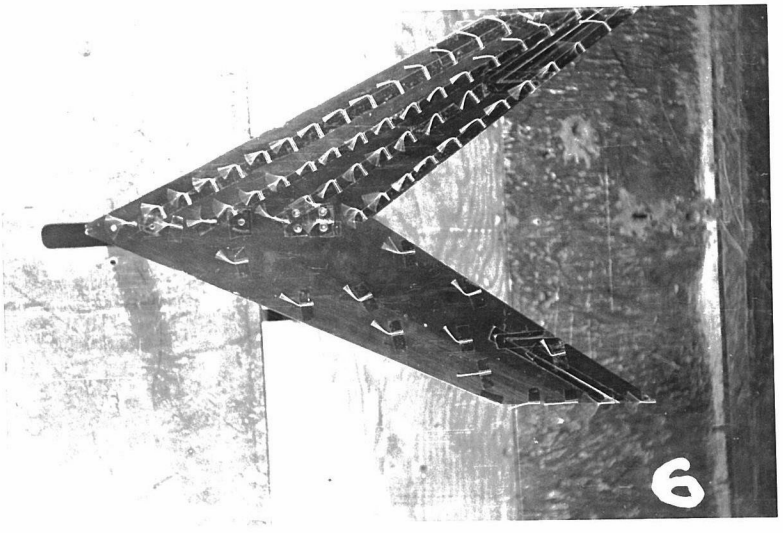

$\alpha = 24°$

Fig. 39

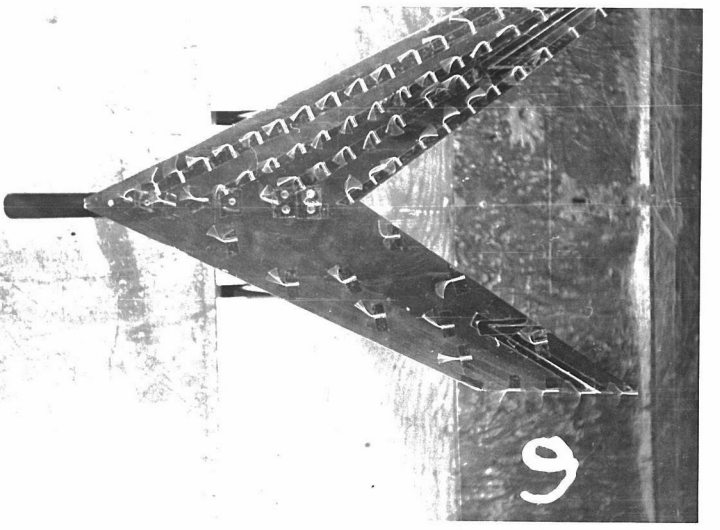

W_s

$\alpha = 34^\circ$

Fig. 40

$W_s B_1 V$

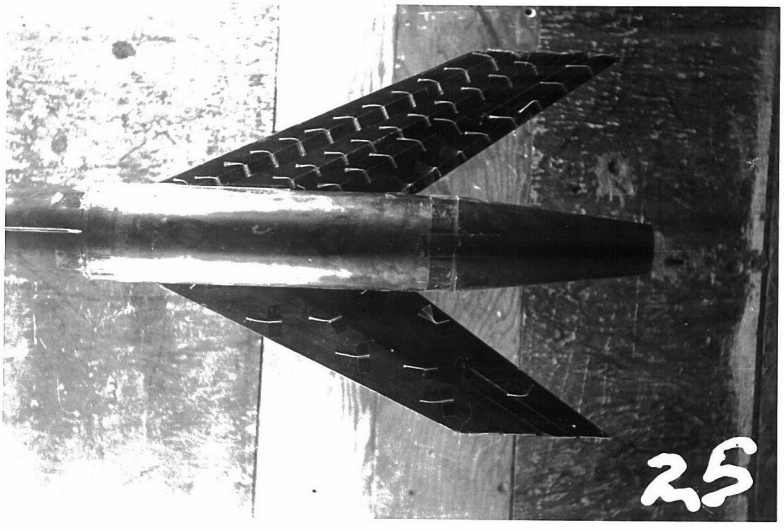

$\alpha = 7°$

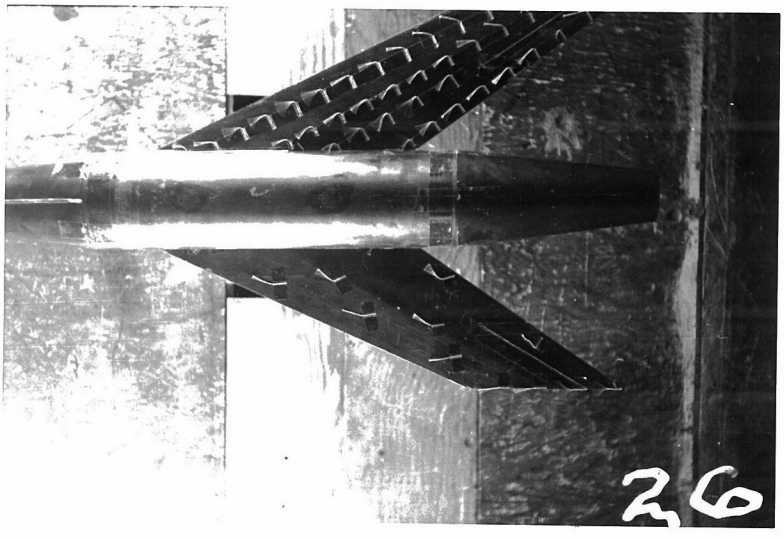

$\alpha = 20°$

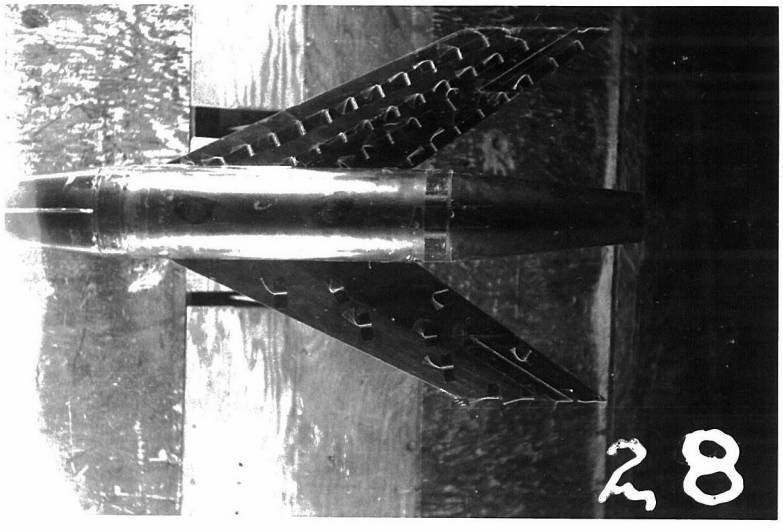

$\alpha = 31°$

Fig. 41

$W_s F_3^{40}$

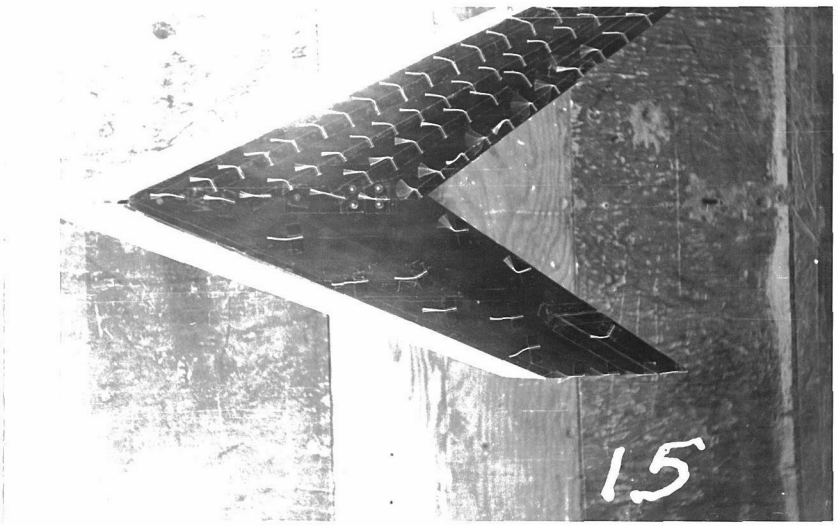

$\alpha = 6°$

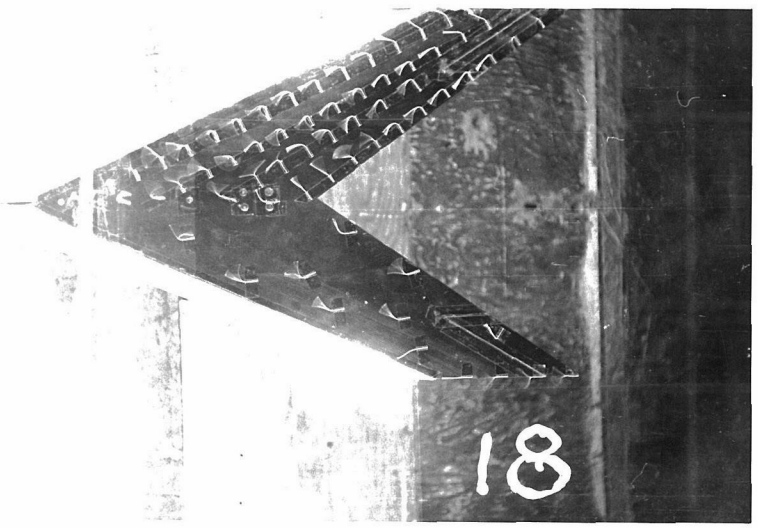

$\alpha = 26°$

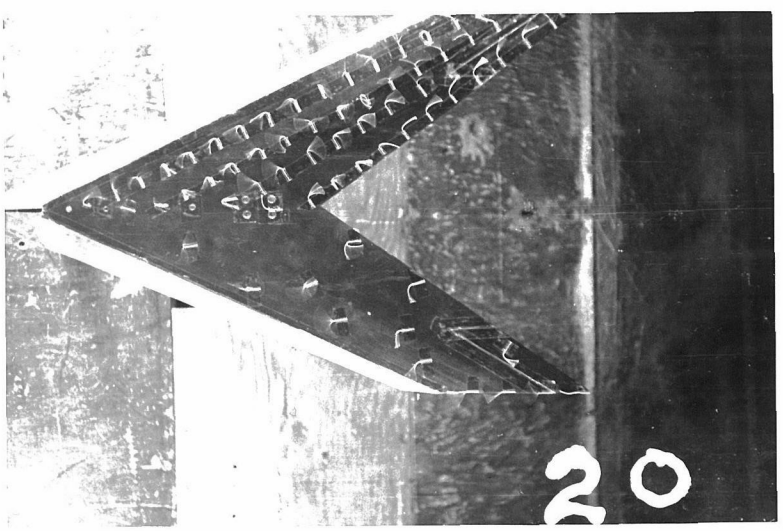

$\alpha = 38°$

Fig. 42

WF_8^{40}

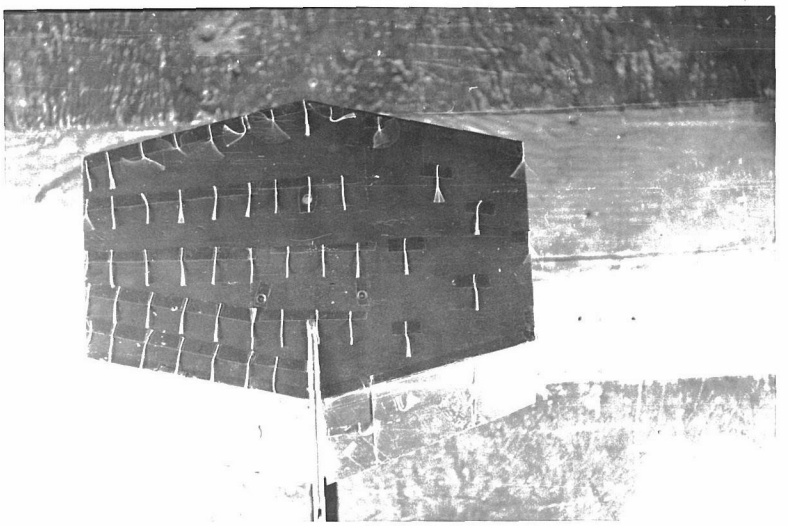

$\alpha = 4°$

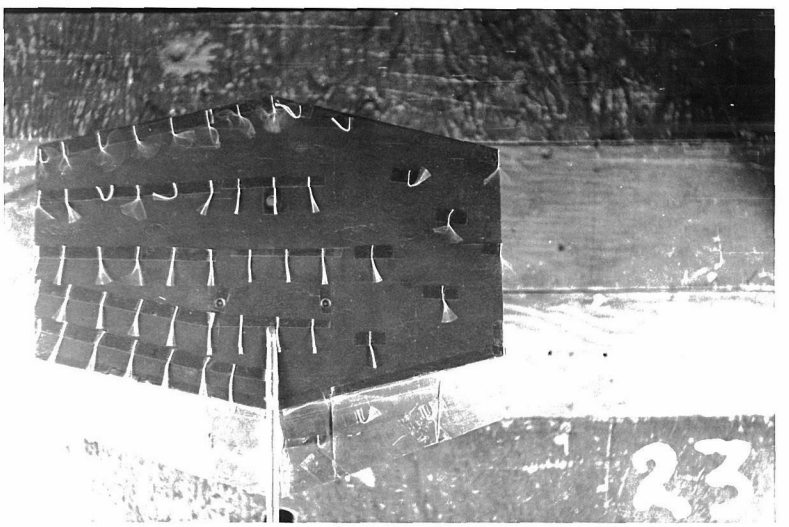

$\alpha = 10°$

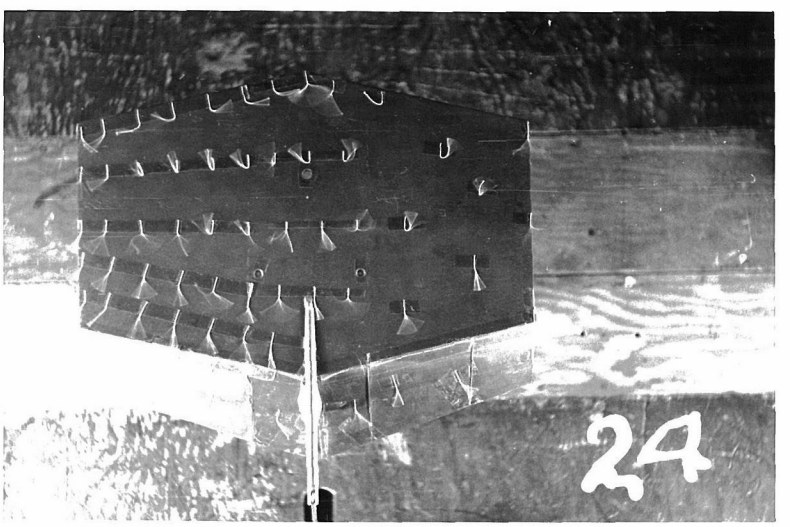

$\alpha = 15°$

Fig. 43

WF_8^{40}

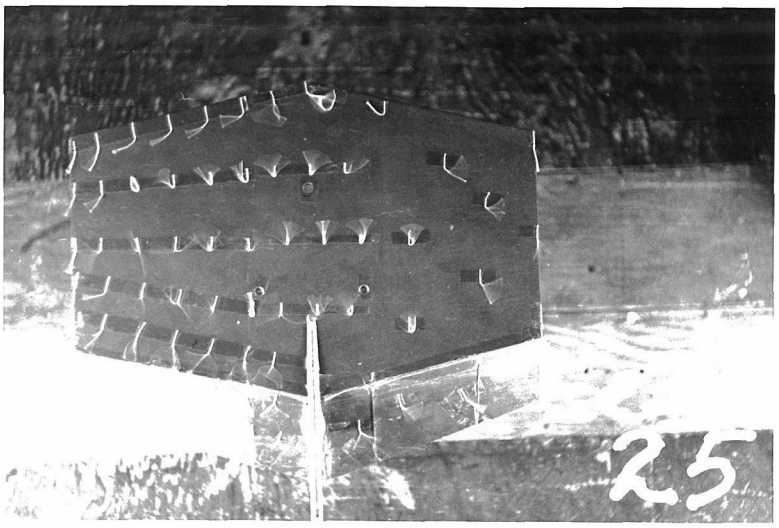

$\alpha = 21°$

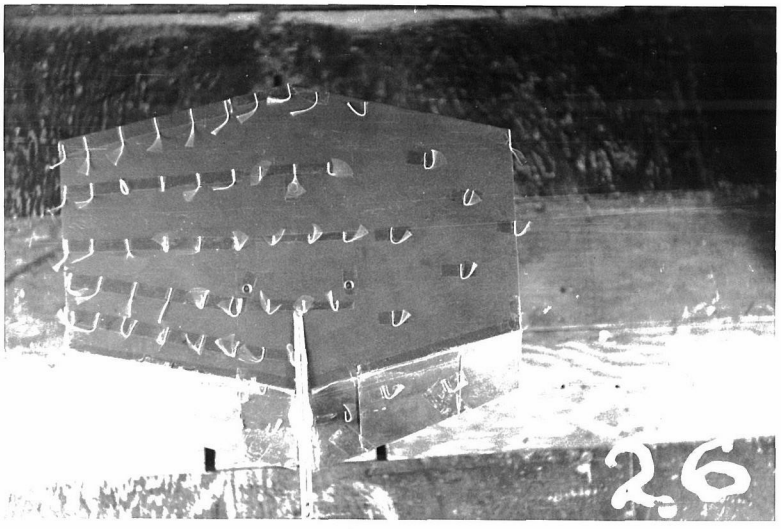

$\alpha = 28°$

Fig. 44

$WF_8(70)^{40}$

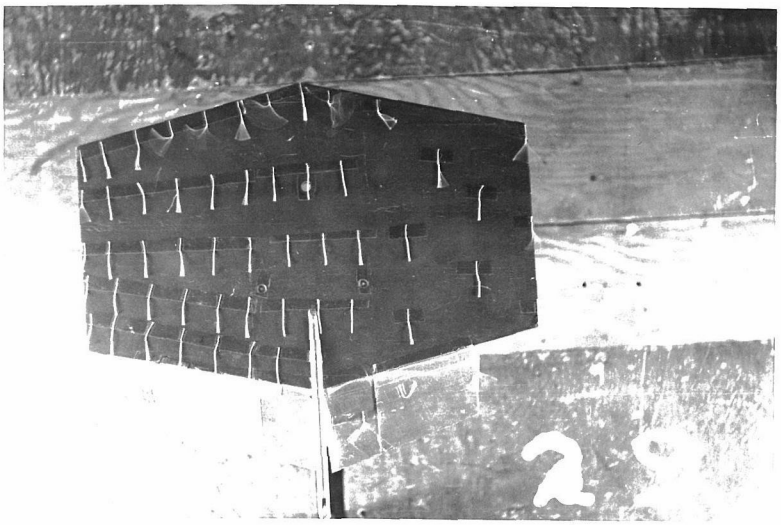

$\alpha = 4°$

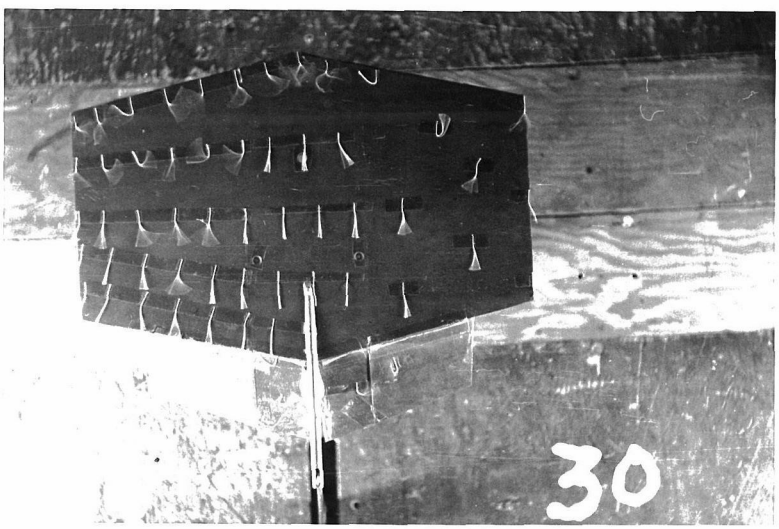

$\alpha = 10°$

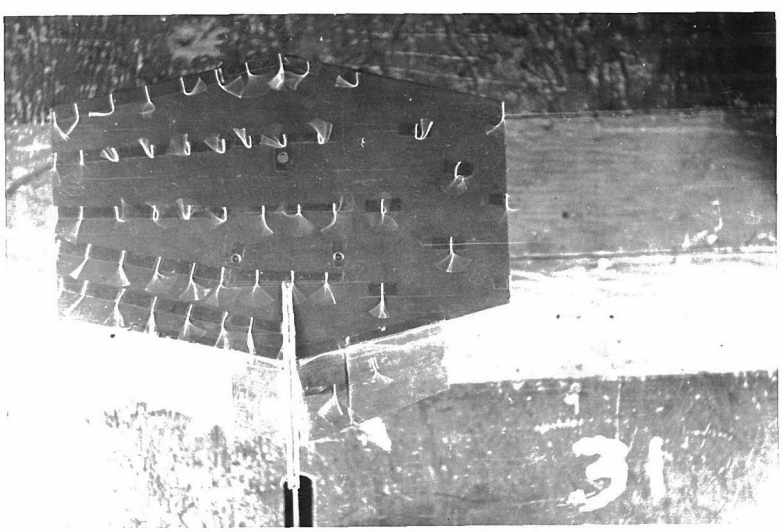

$\alpha = 15°$

Fig. 45

$WF_8(70)^{40}$

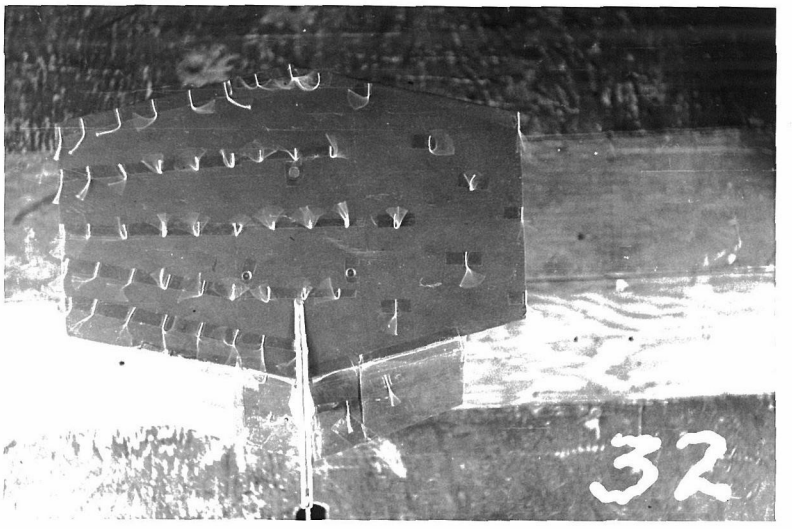

$\alpha = 21^\circ$

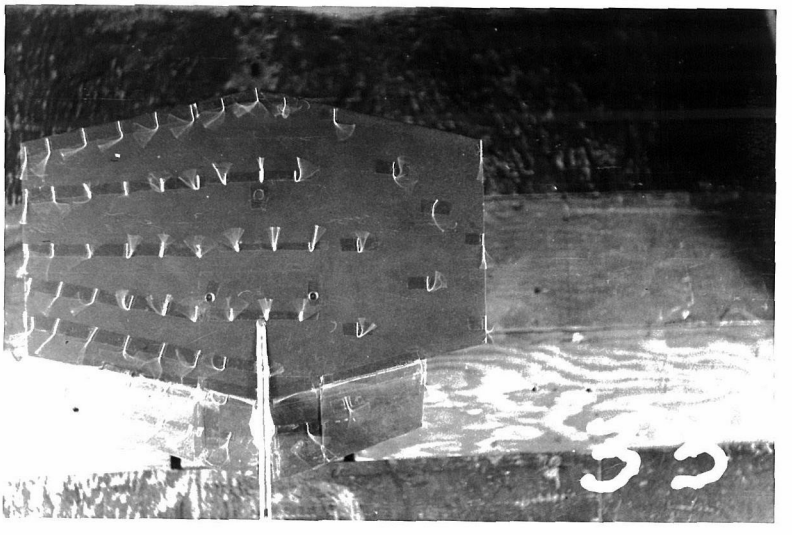

$\alpha = 28^\circ$

$\alpha = 33^\circ$

Fig. 46

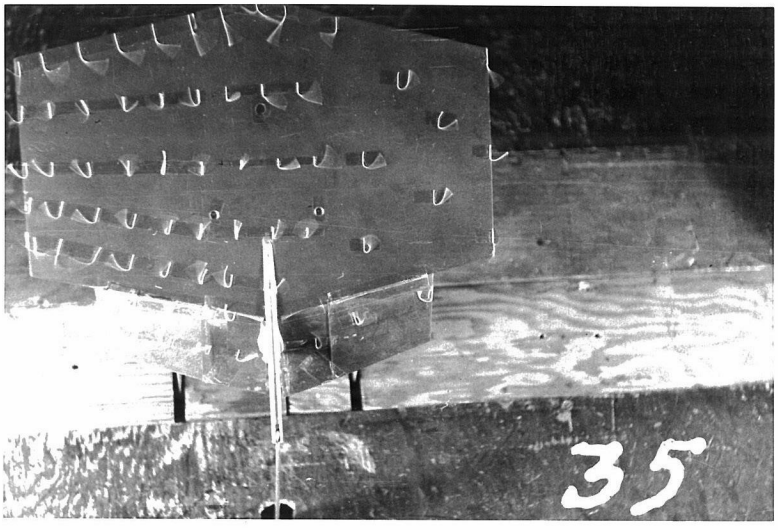

$WF_8(70)^{40}$

$\alpha = 38^\circ$